

RECOMMENDATION ITU-R P.684-2

**Prediction of field strength at frequencies
below about 150 kHz**

(Question ITU-R 225/3)

(1990-1994-2001)

The ITU Radiocommunication Assembly,

considering

- a) that there is a need to give guidance to engineers for the planning of radio services in the frequency band below about 150 kHz;
- b) that the following methods have been developed:
 - a wave-hop treatment for frequencies above about 60 kHz, based on a statistical analysis of field strength measurements in the band 16 kHz to about 1 000 kHz;
 - a waveguide mode method for frequencies below about 60 kHz, based on a theoretical model of the Earth and the ionosphere, employing ionospheric model parameters determined from propagation data;
 - a method for the frequency band 150-1 700 kHz, described in Recommendation ITU-R P.1147,

recommends

1 that the following methods be used, taking particular note of the cautions on accuracy in their application to certain regions as discussed in Annex 2.

1 Introduction

Two methods are available for theoretically calculating the field strength of ELF, VLF and LF signals.

It may be noted that the information in this Recommendation includes values of $f \cos i$ exceeding 150 kHz. The use of this information for frequencies exceeding 150 kHz is not recommended. Recommendation ITU-R P.1147 gives information for frequencies above 150 kHz.

1.1 The wave-hop method is that in which electromagnetic energy paths between a given transmitter and receiver are represented geometrically as is done in the case of HF.

This method should be used at LF and, for distances less than 1 000 km, at VLF. The method treats radio transmission as taking place along certain paths defined by one or more ionospheric reflections, depending on whether the propagation in question involves one or more hops, as well as a ground wave. The total field is then the vectorial resultant of the fields due to each path. In view of the long wavelengths concerned, the diffraction of the waves by the Earth's surface must be taken into account, which is not the case for HF. The wave-hop method may be justified by the fact that, with oblique incidence, the dimensions of the section of altitude in which propagation takes place are equal to or greater than several wavelengths.

With this method it is necessary to know the values of the reflection coefficients of the incident wave on the ionosphere. These vary greatly with frequency, length and geographic and geomagnetic coordinates of transmission path, time of day, season, and epoch of the solar cycle. It is also necessary to know the electrical characteristics (conductivity and permittivity) of the ground at the transmitting and receiving sites, since the finite conductivity of the Earth affects the vertical radiation patterns of the terminal antennas.

1.2 The waveguide mode method should be used at VLF for distances greater than 1 000 km. In this method, the propagation is analysed as the sum of the waves corresponding to each of the different types of propagation in the Earth-ionosphere waveguide, analogous to a mode as defined for waveguides in the microwave region. The selection of the method to be used for field calculation depends on practical consideration of numerical calculations.

1.3 In the case of VLF at distances of less than 1 000 km and for LF in general, the series of modes are slightly convergent and the calculations then require adding together vectorially a large number of components. The wave-hop theory, on the other hand, requires only a limited number of paths, including the ground wave, and it is particularly convenient for the long-distance propagation of LF, taking into account, if possible, the diffraction.

For VLF at distances of more than 1 000 km, the wave-hop theory requires the vectorial addition of the field due to a large number of paths whereas, since the series of modes converge rapidly, sufficient accuracy can be obtained by adding together only a small number of modes. The mode theory, therefore, is better suited to this type of propagation. Propagation at ELF also may be described in terms of a single waveguide mode.

2 Wave-hop propagation theory

2.1 General description

According to this theory, the sky-wave field (strength and phase) at a point is treated as the resultant of the fields created by different waves propagated directly from the transmitter in one or more hops. The total field at this point is then the resultant of the field due to the wave diffracted by the ground and of the field due to the sky wave.

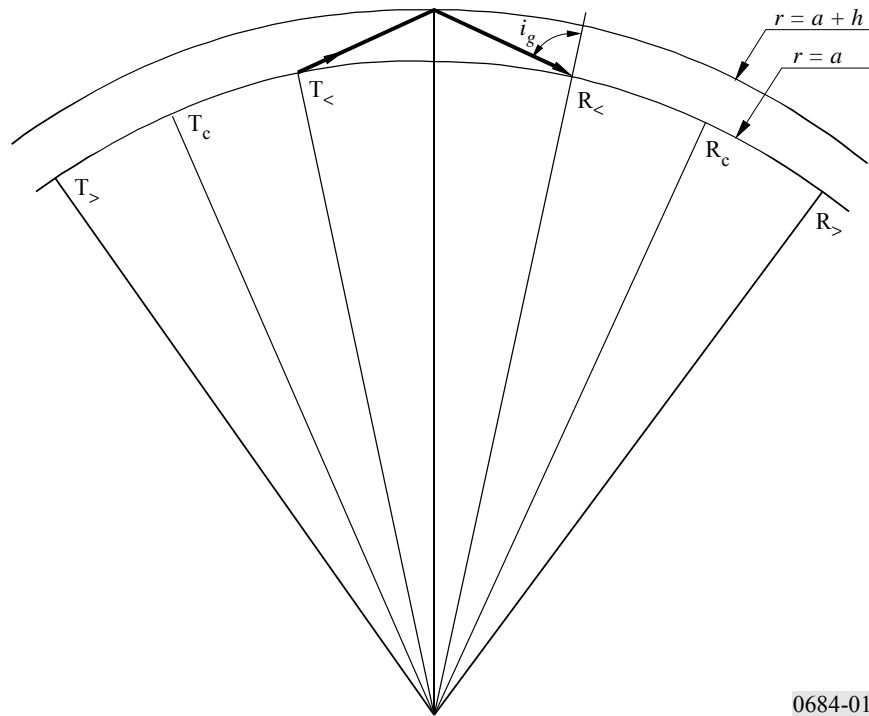
The sky-wave field is calculated by applying the theory of rays in the regions where the methods of geometric optics are applicable and by integrating the effects of diffraction or by applying the full wave theory in regions where optics are no longer valid.

The geometry of a path comprising a single hop is shown in Fig. 1.

The surface of the Earth is defined by $r = a$ and a smooth reflecting ionospheric layer located at $r = a + h$. It is convenient to distinguish three cases. In the first, the receiving antenna located at $R_{<}$ is illuminated by the once-reflected sky wave from the transmitting antenna located at $T_{<}$ where i_g is less than $\pi/2$. In the second, the two antennas at T_c and R_c are located at the critical points where $i_g = \pi/2$. In the third case the antennas are located at $T_{>}$ and $R_{>}$ beyond the critical points such that the first sky-wave hop propagates into the diffraction or shadow zone.

FIGURE 1

Ray path geometry for the wave-hop radio propagation theory (first hop sky wave)



0684-01

2.2 Calculating the ray-path field strength

The electromotive force corresponding to the electric field radiated from a short vertical dipole is given by:

$$V_u = 300 \sqrt{p_t} \quad \text{V} \quad (1)$$

where p_t is radiated power (kW).

The field strength of the downcoming sky wave, before reflection at the ground in the vicinity of the receiving antenna, is given by:

$$E_t = \frac{V_u}{1000L} \cos \psi \parallel R_{\parallel} D F_t \quad \text{mV/m} \quad (2)$$

where:

- L : sky-wave path length (km)
- $\parallel R_{\parallel}$: the ionospheric reflection coefficient which gives the ratio of the electric field components parallel to the plane of incidence
- D : ionospheric focusing factor
- F_t : transmitting antenna factor
- ψ : the angle of departure and arrival of the sky wave at the ground, relative to the horizontal.

If reception is by a small in-plane loop antenna located on the surface of the Earth, the effective field strength of the sky wave is:

$$E_s = \frac{V_u}{500L} \cos \psi \parallel R_{\parallel} D F_t F_r \quad \text{mV/m} \quad (3)$$

For reception by a short vertical antenna equation (3) becomes:

$$E_s = \frac{V_u}{500L} (\cos \psi)^2 \parallel R_{\parallel} D F_t F_r \quad \text{mV/m} \quad (4)$$

where F_r is the appropriate receiving antenna factor.

For propagation over great distances, the wave-hop method can be extended to include sky waves reflected more than once from the ionosphere. For example for a two-hop sky wave, the field strength received by a receiving loop antenna can be represented simply as:

$$E_s = \frac{V_u}{500L} \cos \psi \parallel R_{1\parallel} \parallel R_{2\parallel} D^2 D_G \parallel R_{g\parallel} F_t F_r \quad \text{mV/m} \quad (5)$$

where:

D_G : divergence factor caused by the spherical Earth, approximately equal to D^{-1}

$\parallel R_{g\parallel}$: effective reflection coefficient of the finitely conducting Earth

L : total propagation path of the two-hop ray-path

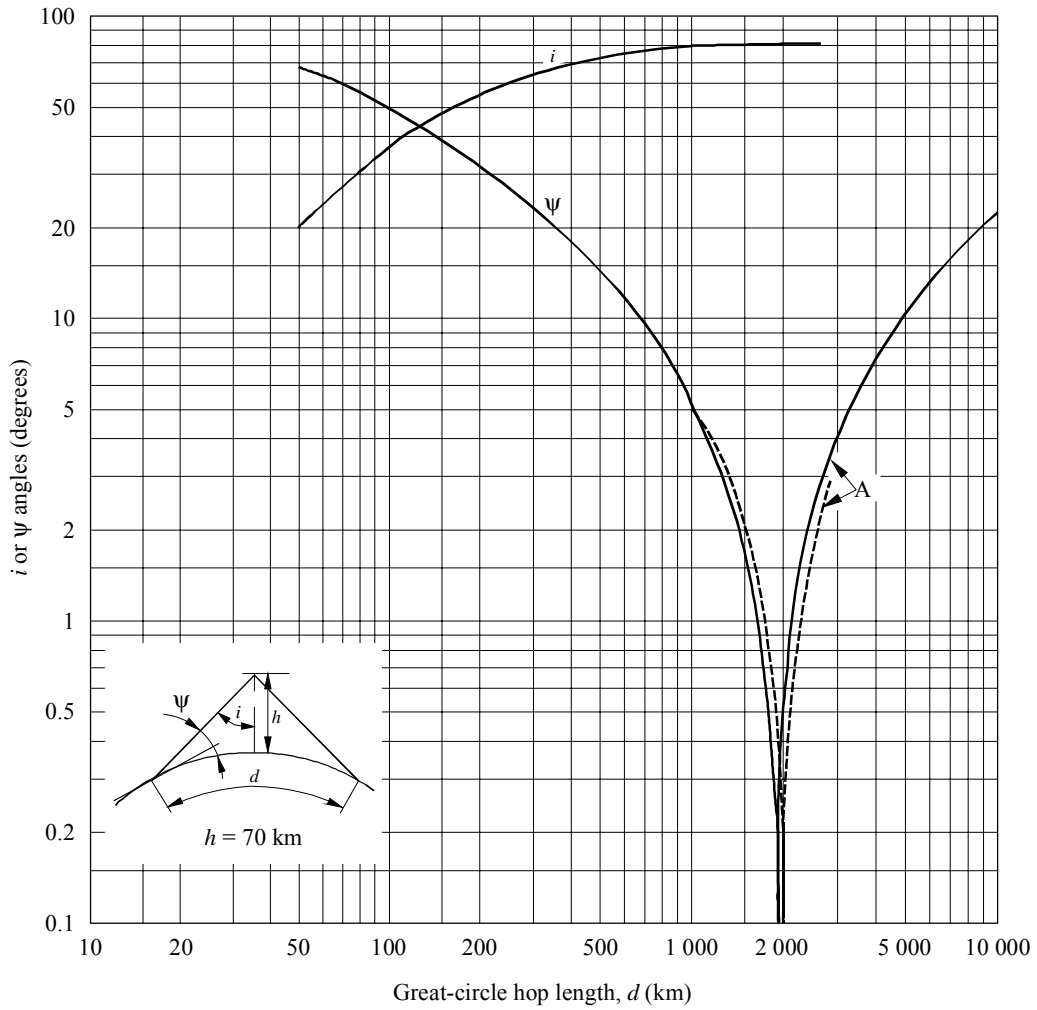
$\parallel R_{1\parallel}$ and $\parallel R_{2\parallel}$: ionospheric reflection coefficients for the first and second reflection.

In general, the ionospheric reflection coefficients will not be equal, because the polarizations of the incident waves are not the same. However, in the simple method for calculating field strengths given here, for propagation at very oblique angles of incidence, $\parallel R_{1\parallel} = \parallel R_{2\parallel}$ as a first order approximation.

2.2.1 Angles of elevation and ionospheric incidence

The ray path geometry for determining the angles of departure and arrival of the sky wave at the ground, ψ , and ionospheric angles of incidence, i , is shown on Figs. 2 and 3. These angles are given in Fig. 2 for an effective reflection height of 70 km which corresponds to typical daytime conditions and in Fig. 3 for an effective reflection of 90 km which corresponds to typical night-time conditions. The effects of atmospheric refraction on the departure and arrival angles are included and shown by the dashed curve although they are probably not valid for frequencies below about 50 kHz.

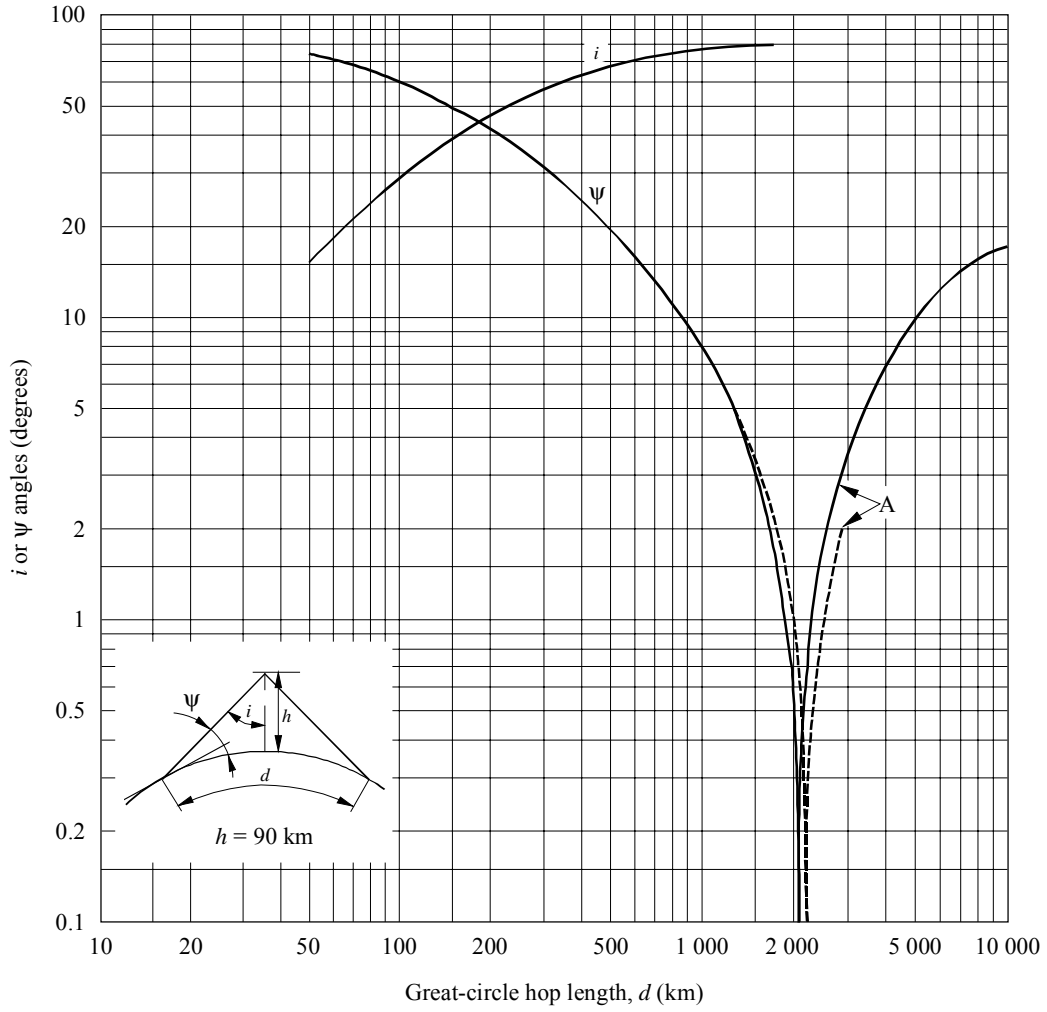
FIGURE 2
 Departure and arrival angles, ψ , and ionospheric angles of incidence, i ,
 for typical daytime conditions ($h = 70$ km). The dashed curve includes
 the effects of atmospheric refraction



A: negative ψ

0684-02

FIGURE 3
 Departure and arrival angles, ψ , and ionospheric angles of incidence, i ,
 for typical night-time conditions ($h = 90$ km). The dashed curve includes
 the effects of atmospheric refraction

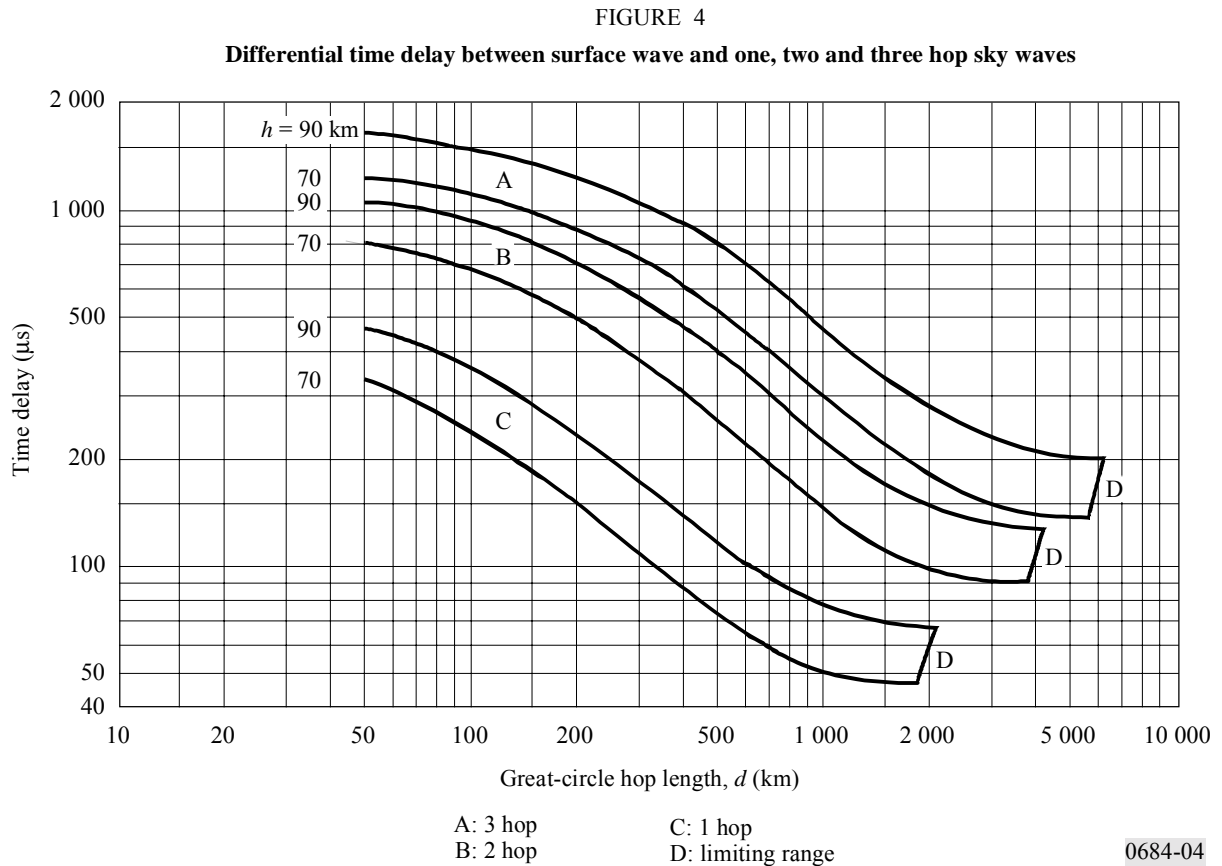


A: negative ψ

0684-03

2.2.2 Path length and differential time delay

To calculate L the sky-wave path length and estimates of the diurnal phase changes, Fig. 4 is used. This shows the differential time delay between the surface wave and the one, two or three hop sky wave for ionospheric reflection heights of 70 and 90 km, corresponding to daytime and night-time conditions. A propagation velocity of 3×10^5 km/s is assumed.



2.2.3 Focusing factor

The ionospheric focusing factor, D , for a spherical Earth and ionosphere is shown in Fig. 5 for daytime conditions and in Fig. 6 for night-time conditions.

2.2.4 Antenna factors

The antenna factors, F_t and F_r , which account for the effect of the finitely conducting curved Earth on the vertical radiation pattern of the transmitting and receiving antennas are shown in Figs. 7 to 9. Factors are calculated for land, sea and ice conditions which are defined by their electrical characteristics (conductivity and permittivity), as shown in Table 1.

FIGURE 5
Ionospheric focusing factor – daytime

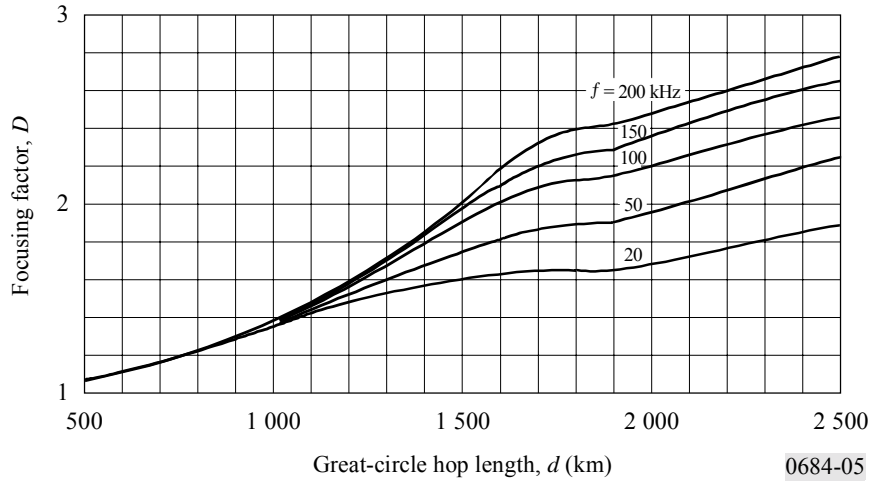


FIGURE 6
Ionospheric focusing factor – night-time

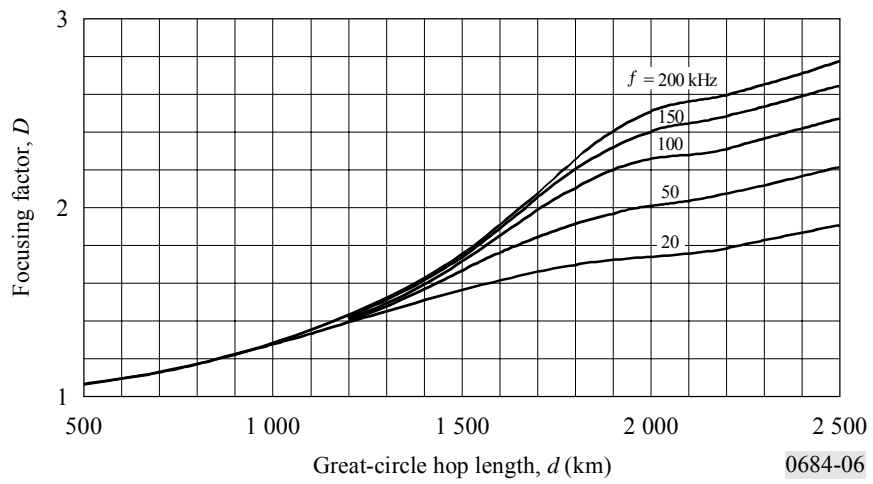
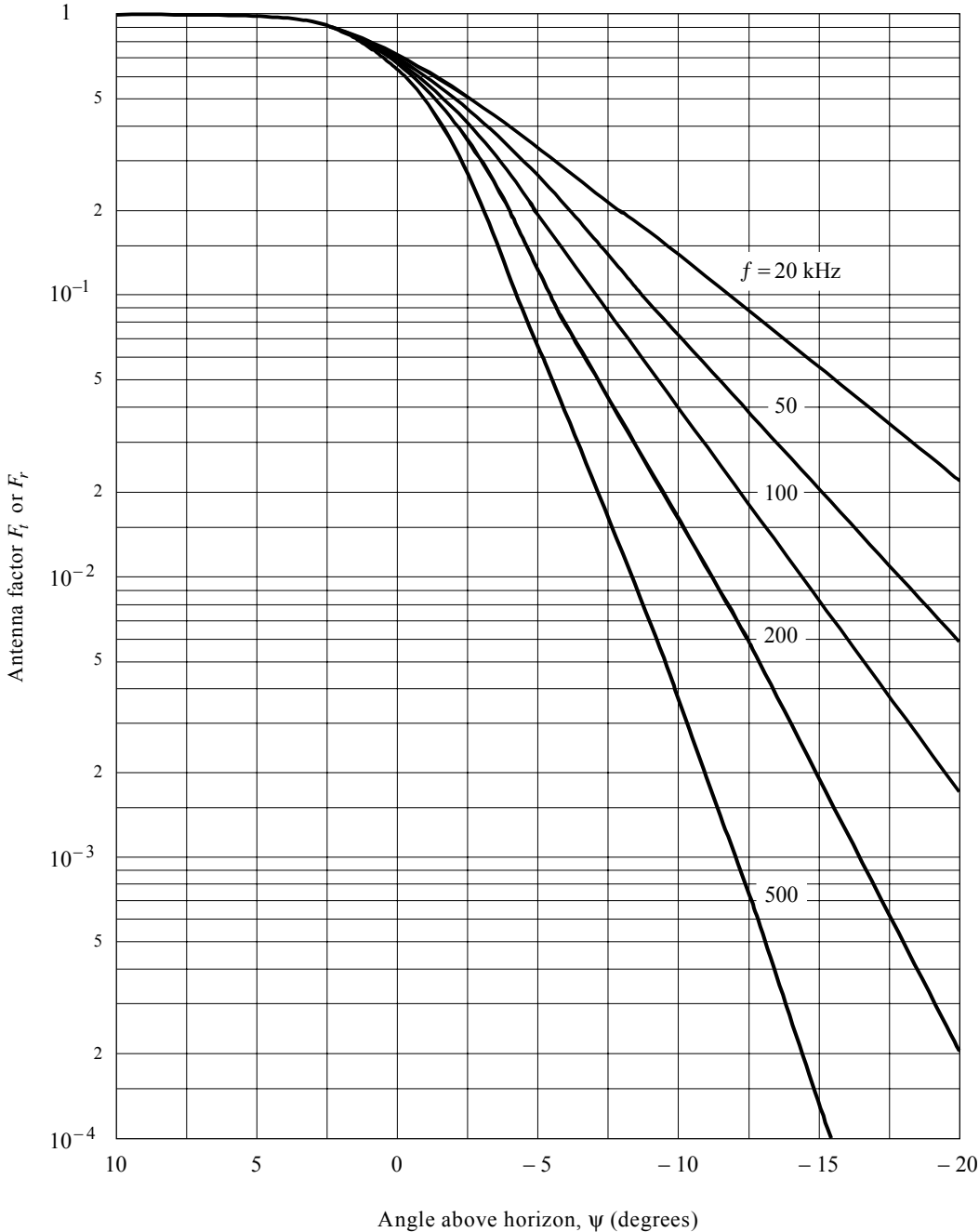


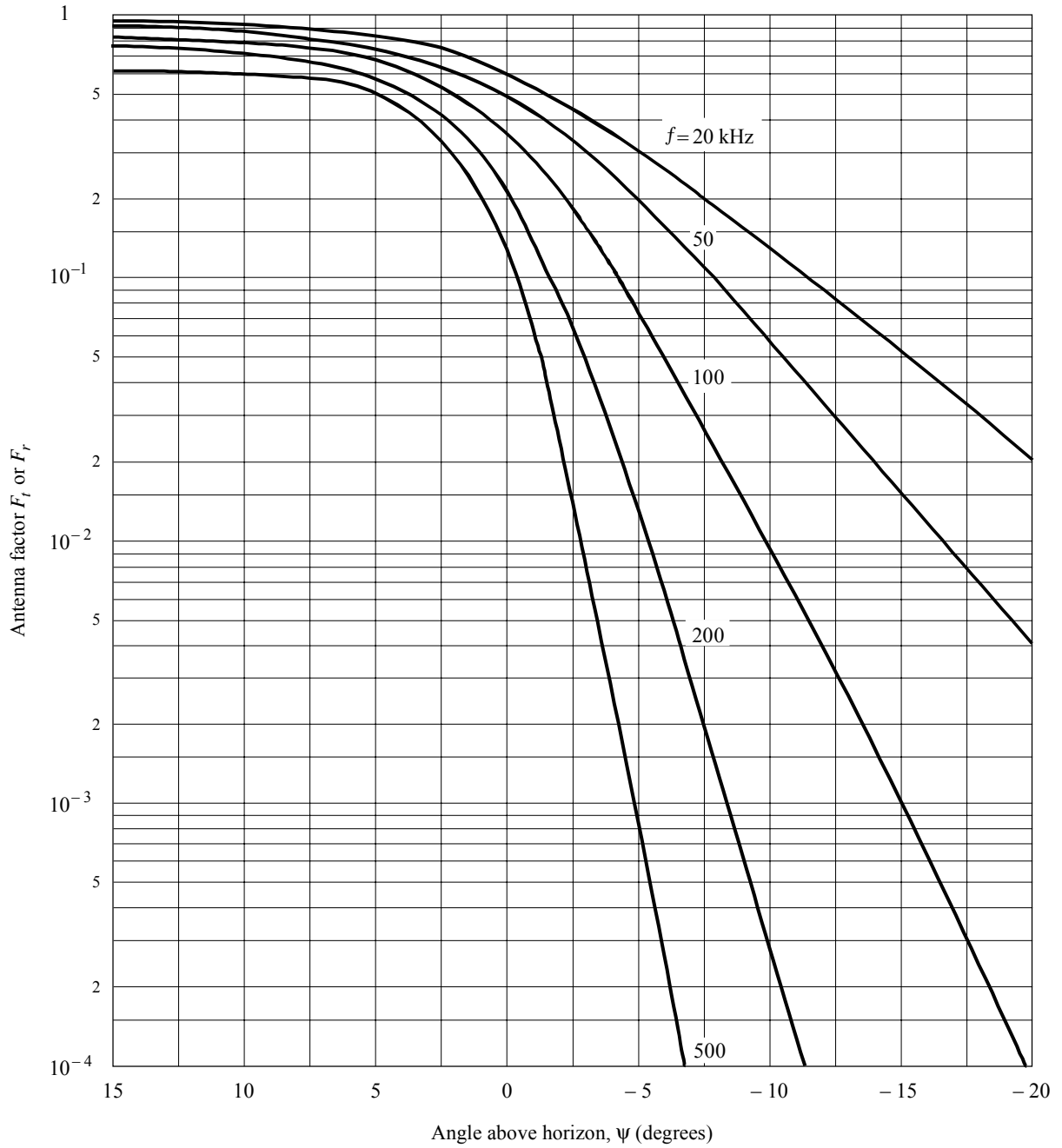
FIGURE 7
Antenna factor – Sea water



$\epsilon = 80 \epsilon_0$
 $\sigma = 5 \text{ S/m}$
 $\alpha = 4/3 \times 6\,360 \text{ km}$

0684-07

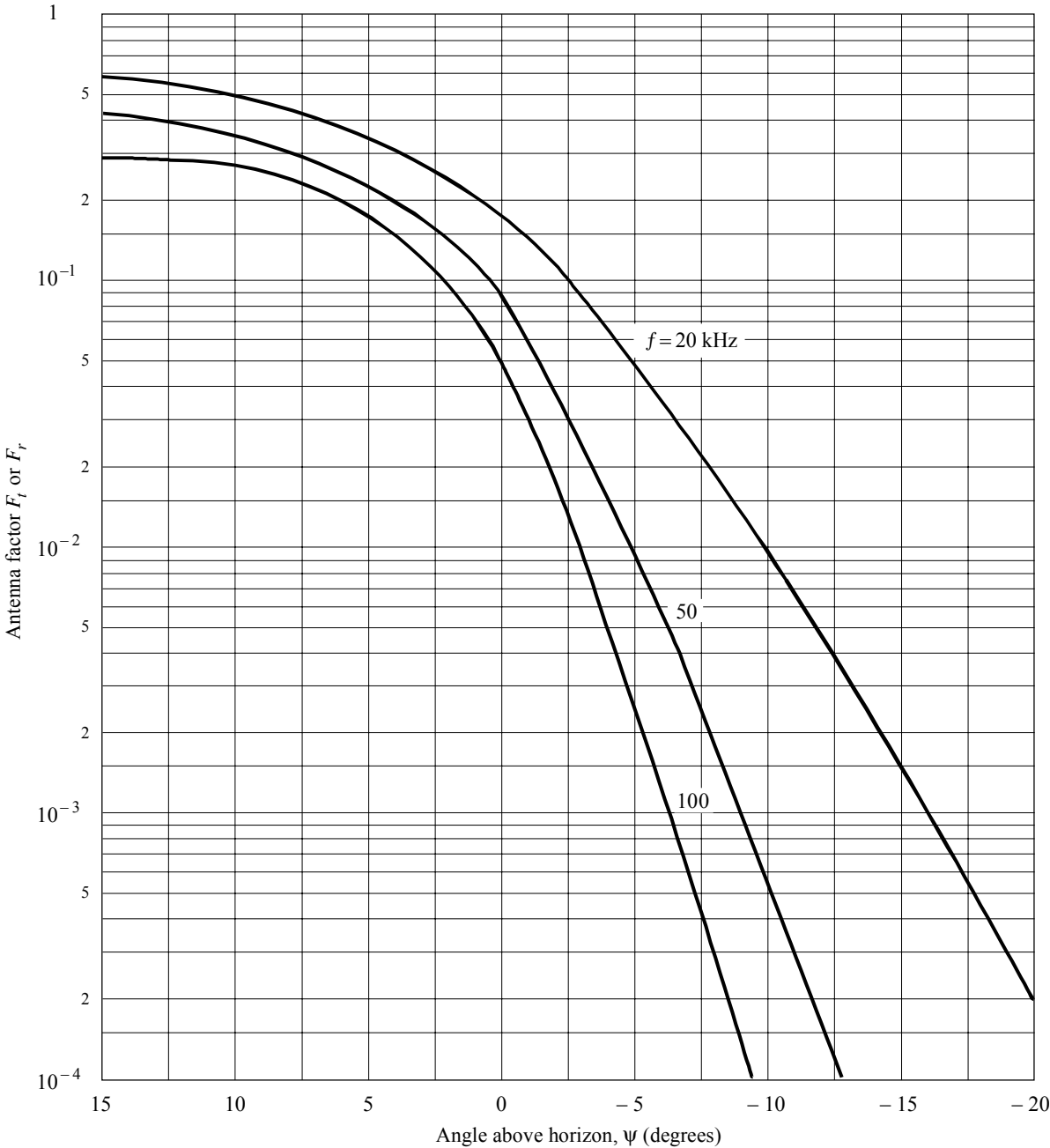
FIGURE 8
Antenna factor – Land



$\epsilon = 15 \epsilon_0$
 $\sigma = 2 \times 10^{-3} \text{ S/m}$
 $\alpha = 4/3 \times 6360 \text{ km}$

0684-08

FIGURE 9
Antenna factor – Ice at -4° C



$\epsilon = 3 \epsilon_0$
 $\sigma = 0.025 \times 10^{-3} \text{ S/m}$
 $\alpha = 4/3 \times 6360 \text{ km}$

0684-09

TABLE 1

	Conductivity, σ (S/m)	Permittivity, ϵ
Sea water	5	$80 \epsilon_0$
Land	2×10^{-3}	$15 \epsilon_0$
Polar ice	2.5×10^{-5}	$3 \epsilon_0$

ϵ_0 : permittivity of free space

The curves were calculated assuming an effective Earth's radius, 8 480 km, which is 4/3 of its actual value to take account of atmospheric refraction effects. The factors F are the ratio of the actual field strength to the field strength that would have been measured if the Earth were perfectly conducting. Negative values of ψ refer to propagation beyond the geometric optical limiting range for a one hop sky wave (see Figs. 1 to 3).

2.2.5 Ionospheric reflection coefficients ${}_{\parallel}R_{\parallel}$

Values of the ionospheric reflection coefficient ${}_{\parallel}R_{\parallel}$ are shown in Fig. 10 for solar cycle minimum. To take account of frequency and distance changes, the values of ${}_{\parallel}R_{\parallel}$ are given as a function of $f \cos i$, where f is the transmitted frequency and i is the ionospheric angle of incidence. Curves are shown for night during all seasons, and for day conditions during winter and summer. Measured values at vertical and oblique incidence are indicated based upon the results given in numerous reports.

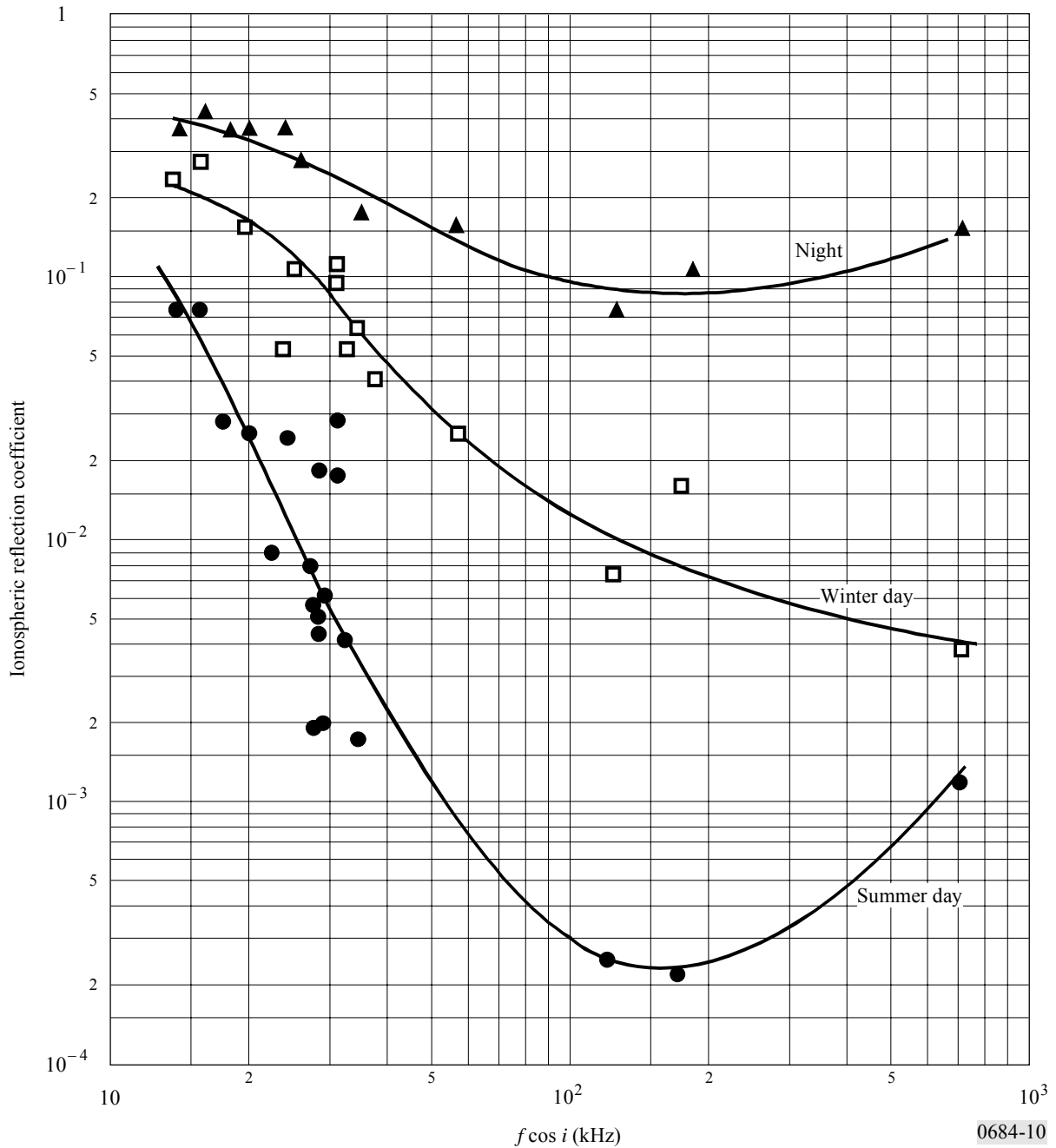
In all cases the ionospheric reflection coefficient data given in the various references mentioned have been modified, if necessary, to account for ionospheric focusing, antenna factors, etc., so that the results of the measurements are consistent with the analysis technique given here.

The concept of an effective frequency $f \cos i$ for which reflection coefficients are constant cannot, however, always be relied on. The curves in Fig. 10 are derived from data obtained at steep incidence ($d < 200$ km) and at more oblique incidence ($d > 500$ km) and the $f \cos i$ concept is likely to be approximately correct for such distances. At intermediate distances, however, the concept of an equivalent frequency is likely to lead to substantial errors in reflection coefficient, because in such circumstances the reflection coefficient and polarization of the wave change rapidly with distance.

While many data have been incorporated into the curves in Fig. 10, which show that the ionospheric reflection coefficient varies with time of day (midnight and noon) and season, much more work is needed to establish clearly how it varies over the epoch of the solar cycle. There is clearly a solar cycle variation (see Fig. 11) in that reflection coefficients are larger in sunspot maximum years at the very low frequencies, whereas at medium frequencies they are smaller. The physical interpretation of this fact is as follows. During sunspot maximum years, the base of the ionosphere is lower and the electron density gradient is steeper than during sunspot minimum years. Thus, VLF waves which are reflected from this lower layer are more strongly reflected in sunspot maximum years, whereas MF waves, that are reflected above this lower layer, are more strongly absorbed. Clearly, the transition between greater and smaller reflection coefficients would be expected to be a function of frequency, time of day, season and epoch of the solar cycle; and a discontinuity in the

reflection coefficient-frequency curve, at some particular frequency and time might be expected. A sharp change in the values for effective frequencies of 35 to 45 kHz is apparent in the data for sunspot maximum years in summer, but this is not revealed in the presentation of the data here.

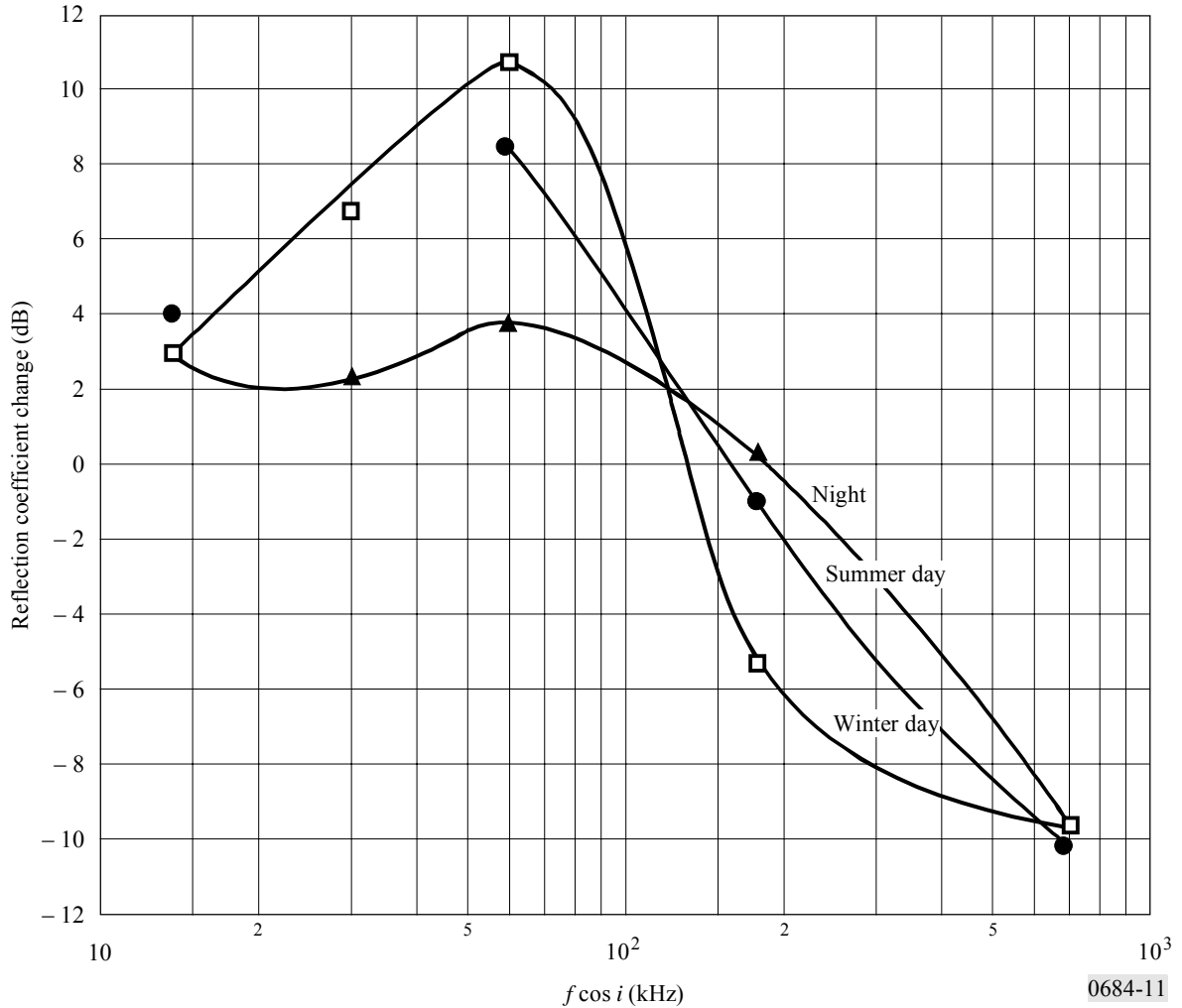
FIGURE 10
Ionospheric reflection coefficients – solar minimum conditions



It should be noted that the frequency range of the MF broadcast band for oblique propagation lies in the range of effective frequencies where the solar cycle change in ionospheric reflectivity is opposite. That is, 1 600 kHz propagated over a path of 1 500 km corresponds to a $f \cos i$ of 278 kHz; whereas at 500 kHz the effective frequency is 86 kHz. An example of a calculation by the ray-path method is given in Annex 1.

FIGURE 11

Change in reflection coefficient (dB) from sunspot minimum to maximum years as a function of effective frequency and time



3 Calculating field strength by waveguide modes: full wave solution

In the propagation of ELF, VLF and LF terrestrial radio waves to great distances, the waves are confined within the space between the Earth and the ionosphere. This space acts as a waveguide and the “waveguide concept” is applicable for characterizing the propagated fields as a function of distance.

The waveguide mode method obtains the full wave solution for a waveguide that has the following characteristics:

- arbitrary electron and ion density distributions and collision frequency (with height), and
- a lower boundary which is a smooth homogeneous Earth characterized by an adjustable surface conductivity and dielectric constant. This method also allows for Earth curvature, ionospheric inhomogeneity, and anisotropy (resulting from the Earth’s magnetic field).

The energy within the waveguide is considered to be partitioned among a series of modes. Each mode represents a resonant condition, i.e., for a discrete set of angles of incidence of the waves on the ionosphere, resonance occurs and energy will propagate away from the source. The complex angles (θ) for which this occurs are called the eigenangles (or “modes”). They may be obtained using the “full-wave” procedures described in § 3.1 and 3.2 by solving the determinantal equation (i.e. the modal equation):

$$F(\theta) = |R_d(\theta) \bar{R}_d(\theta) - 1| = 0 \quad (6)$$

where:

$$R_d(\theta) = \begin{bmatrix} {}_{\parallel}R_{\parallel d}(\theta) & {}_{\perp}R_{\parallel d}(\theta) \\ {}_{\parallel}R_{\perp d}(\theta) & {}_{\perp}R_{\perp d}(\theta) \end{bmatrix} \quad (7)$$

is the complex ionospheric reflection coefficient matrix looking up into the ionosphere from height “ d ” and:

$$\bar{R}_d(\theta) = \begin{bmatrix} {}_{\parallel}\bar{R}_{\parallel d}(\theta) & 0 \\ 0 & {}_{\perp}\bar{R}_{\perp d}(\theta) \end{bmatrix} \quad (8)$$

is the complex reflection matrix looking down from height “ d ” towards the ground.

The notation \parallel for the R 's and \bar{R} 's denotes vertical polarization while the notation \perp , denotes horizontal polarization. The first subscript on the R 's refers to the polarization of the incident wave while the second applies to the polarization of the reflected wave.

The individual terms of equations (7) and (8) are:

- ${}_{\parallel}R_{\parallel}$: ratio of the reflected field in the plane of incidence to the incident field in the same plane
- ${}_{\perp}R_{\perp}$: ratio of the reflected field perpendicular to the plane of incidence to the incident field perpendicular to the plane of incidence
- ${}_{\parallel}R_{\perp}$: ratio of the reflected field perpendicular to the plane of incidence to the incident field in the plane of incidence
- ${}_{\perp}R_{\parallel}$: ratio of the reflected field in the plane of incidence to the incident field perpendicular to the plane of incidence

The ionospheric reflection matrix, R_d (equation (7)) at height, d , is obtained by numerical integration of differential equations given by Budden (“The waveguide theory of wave propagation”, Logos Press, London, 1961). The differential equations are integrated by a Runge-Kutta technique, starting at some height above which negligible reflection is assumed to take place. The initial condition for the integration, i.e. the starting value of R , is taken as the value of R for a sharply-bounded ionosphere at the top of the given electron density and collision frequency profiles. The term R_d is calculated in terms of solutions to Stokes equation and their derivatives.

The modal equation, equation (6), is solved for as many modes (eigenangles, θ_n) as desired. From the set of θ 's so obtained the propagation parameters: attenuation rate, phase velocity and the magnitude and phase of the excitation factor, can be computed. These parameters are then used in a modal summation to compute the total field, amplitude and phase, at some distant point.

In many instances, the Earth-ionosphere waveguide can be considered to have constant propagation properties along the transmission path. The mode sum calculations made for these cases are referred to as horizontally homogeneous. However, for propagation to great distances it is unrealistic to assume the waveguide parameters will remain constant along the whole length of the path. For example, the direction and strength of the Earth's magnetic field will vary and discontinuities can occur in the lower wall of the waveguide due to the presence of ground conductivity changes associated with various land-sea boundaries and the polar ice caps. The ionospheric conductivity also varies according to the time of day, season and the presence of the sunrise or sunset line along the propagation path.

These types of discontinuities are those which cause discrete changes in the waveguide. In these cases mode conversion effects at the discontinuity must be taken into consideration. Mode conversion implies that a single mode propagating in one region of the waveguide will produce two or more modes in the other section of the guide which then propagate to the receiver.

3.1 The ionospheric reflection matrix, $R(\theta)$

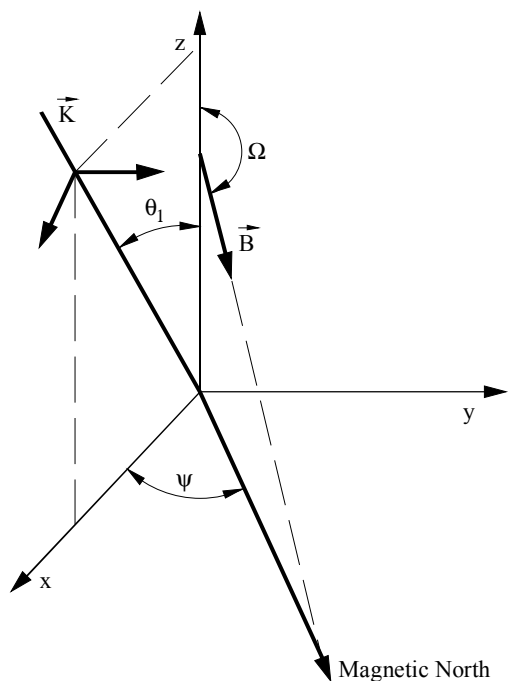
A crucial step in the determination of the mode constants discussed in the previous section is the evaluation of the reflection matrix R for a vertically inhomogeneous anisotropic ionosphere. This is achieved by a numerical integration of differential equations given by Budden.

The coordinate system chosen is such that the direction of z is taken as positive into the ionosphere. Positive x is the direction of the propagation and y is normal to the plane of propagation.

The geometry is shown in Fig. 12 where a plane wave is shown incident upon the ionosphere from below with wave vector \vec{K} in the x - z plane (plane of incidence) at an angle of incidence θ_1 to the vertical (z -axis). Other variables identified in the Figure are Ω , the angle of the geomagnetic field measured from the vertical ($90^\circ < \Omega \leq 180^\circ$ for the Northern Hemisphere), and ψ , the azimuth of propagation (East of magnetic North). The vector \vec{B} is the Earth's magnetic flux density.

The differential equations are integrated by a Runge-Kutta technique starting at some height above which negligible reflection is assumed to take place. The starting value of R is the value of R for a sharply bounded homogeneous ionosphere characterized by parameters at the top of the given electron, ion and collision frequency profiles. Error control in the Runge-Kutta integration is by means of comparison for each step of the increments in the elements of R computed with a fourth-order Runge-Kutta method and those computed with a second-order integration step. The integration is carried out from some starting height down to the height d , where d is identified in equation (6). It is necessary only that d be chosen sufficiently low in the ionosphere that ionospheric effects are small relative to Earth-curvature effects. Below level d the only effect is that of Earth curvature which is included by introducing a modified permittivity which varies linearly in height.

FIGURE 12
Wave propagation geometry



0684-12

3.2 The ground reflection matrix, $\bar{R}_d(\theta)$

The ground reflection coefficient matrix, \bar{R}_d , as given in equation (8), is determined in terms of independent solutions, h_1 and h_2 to Stokes' equation

$$\frac{d^2 h_{1,2}}{dz^2} + zh_{1,2} = 0 \quad (9)$$

where the functions h_1 and h_2 are modified Hankel functions of order 1/3 (which are linearly related to Airy functions).

3.3 The mode finding method ("MODESRCH")

Waveguide theory treats the field as being composed of one or more discrete families (modes) of plane waves confined to the Earth-ionosphere waveguide. The principal objective is to find solutions to equation (6) for the eigenangles θ_n . To achieve this a method known as "MODESRCH" is employed.

The "MODESRCH" method, developed primarily for VLF and lower LF (10 kHz to about 60 kHz) propagation in the Earth-ionosphere waveguide finds all modes in any physically important rectangular region of the complex eigenangle (θ_n) space. The method also finds the single mode needed for ELF propagation. The procedure is based on complex variable theory. The modal equation, equation (6), is solved for all the important eigenangles, θ_n , for the given set of Earth-ionosphere parameters and propagation frequency. The search for the eigenangles is based on the fact that the lines of constant phase for any complex function, $F(\theta)$, may be discontinuous only

at points where $F(\theta) = 0$ or $F(\theta) \rightarrow \infty$. To simplify the problem of finding the θ_n values, the function $F(\theta)$ is modified so that it contains no poles and only $F(\theta) = 0$ is considered. A solution of $F(\theta) = 0$ is denoted by θ_0 , i.e. θ_0 is a zero of $F(\theta) = 0$.

Let:

$$F(\theta) = F_R(\theta_r, \theta_i) + j F_I(\theta_r, \theta_i) = \text{Re}(F) + j \text{Im}(F) \quad (10)$$

where:

$$\theta = \theta_r + j \theta_i \quad (11)$$

Also:

$$F(\theta) = \left[(F_R(\theta_r, \theta_i))^2 + (F_I(\theta_r, \theta_i))^2 \right]^{1/2} e^{j\phi} \quad (12)$$

where:

$$\phi = \text{tg}^{-1} \left[\frac{F_I(\theta_r, \theta_i)}{F_R(\theta_r, \theta_i)} \right] \quad (13)$$

and:

$F_R(\theta)$: real part of the complex function $F(\theta)$

$F_I(\theta)$: imaginary part of the complex function $F(\theta)$

θ_r : real part of the complex angle θ

θ_i : imaginary part of the complex angle θ .

From equation (13) if:

$\phi = 0^\circ$ (or 180°), this implies that

$$F_I(\theta_r, \theta_i) = 0$$

Also if:

$\phi = 90^\circ$ (or 270°), this implies that

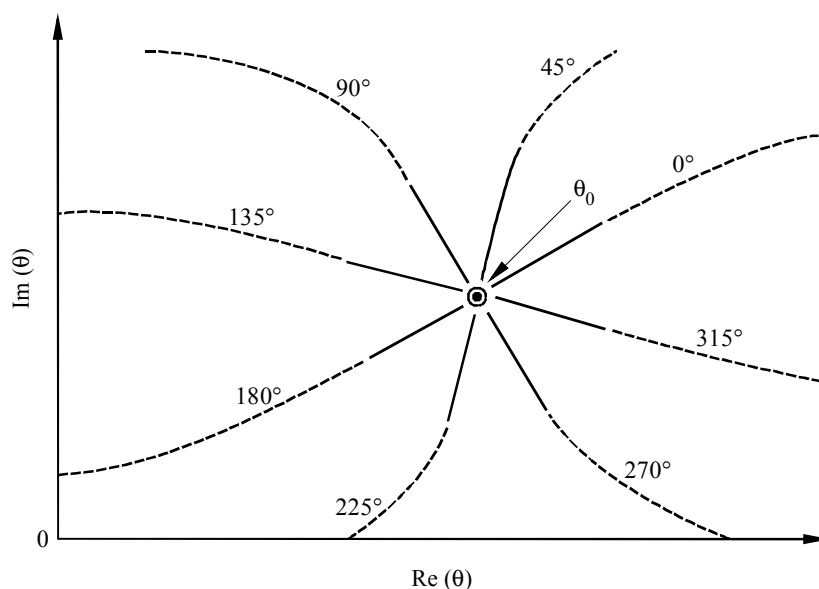
$$F_R(\theta_r, \theta_i) = 0$$

This leads to the phase diagram of Fig. 13. A set of lines of constant phase referred to as phase contours ranging from 0 to 2π radians emanates radially (solid lines) from a simple zero. The dashed lines depict possible phase contour behaviour, in the region beyond the neighbourhood of θ_0 , in order to emphasize that in this region the phase contours are generally not radial. In view of the phase behaviour near a zero of $F(\theta)$ it is conceptually useful to define a zero of $F(\theta)$ as a set of phase contours.

Some fundamentals of the procedure to find zeros of the function, $F(\theta)$, are illustrated in Fig. 14. A search rectangle is placed about some region of the complex plane. The search rectangle is divided into a grid of mesh squares whose corners will be called mesh points. The mesh square size is optional and is usually selected according to the expected zero spacing. If $F(\theta)$ has no poles, this implies that the line of any particular constant phase value $\phi = \phi_c$, radiating from a zero of $F(\theta)$, must cross a closed contour containing that zero at least once. Furthermore, no other zero of $F(\theta)$ may be on this phase line. Also, the lines of constant phase around $F(\theta) = 0$ progress only in an anti-clockwise direction. A line of constant phase (e.g. $\phi = \phi_c$) which crosses the contour may be followed inward until it leads to a zero of $F(\theta)$ or until the line again reaches the contour. Beginning

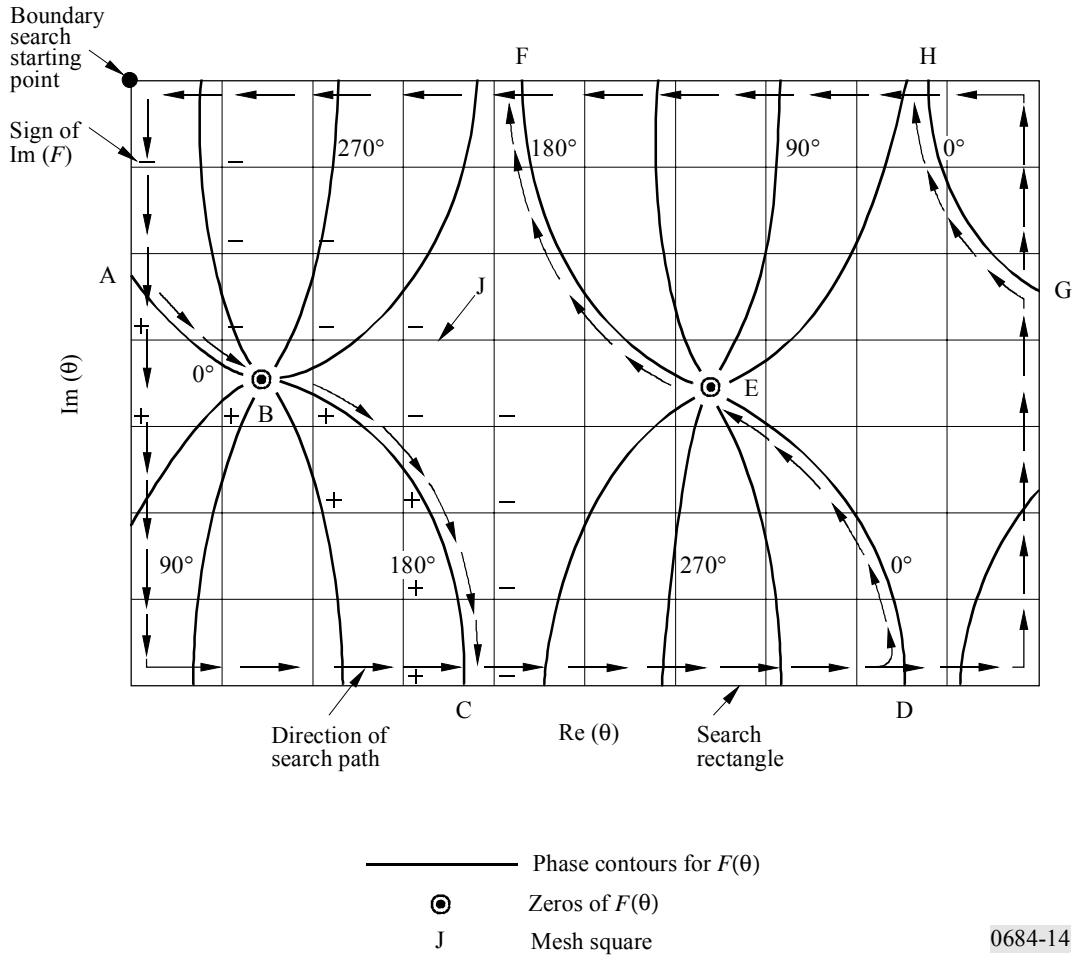
at the upper left corner of the search rectangle, a boundary search for 0° and 180° phase contours is conducted in a counterclockwise direction. Any phase contour would do; however, the 0° and 180° phase contours are selected because mathematically they are easily located, occurring when $\text{Im}(F) = 0$. The search is conducted by evaluating $F(\theta)$ at the mesh points along the search rectangle boundary. When $\text{Im}(F)$ changes sign, it indicates that a 0° or 180° phase contour has just been passed (points A, D, and G). Once either of these phase contours is located, the boundary search is temporarily halted while the 0° or 180° phase contour is traced into the interior of the search rectangle by inspection of $\text{Im} F(\theta)$ at the corners of the mesh squares (counterclockwise inspection beginning at the top left corner of each mesh square). The phase contour is followed either until a zero of $F(\theta)$ is discovered (points B and E) or until the search rectangle boundary is encountered (as would be the case for the phase contour between G and H), one of which will always occur provided no poles exist in the interior of the search rectangle. When a zero is located its location is saved. Then the phase contour is traced out the opposite side of the zero, having undergone a 180° phase change (see Fig. 13), until the search rectangle boundary is again encountered (points C and F). When the phase contour exists the search boundary, such as at points C, F, or H, the mesh square which contains this occurrence is flagged so as to avoid following the particular phase contour again at a later time during the boundary search. Also at such a point (point C, F, or H) the phase contour trace is stopped and the boundary search is resumed at the point where the last 0° or 180° phase line was encountered (e.g. points A, D, or G). Once the entire search rectangle boundary has been inspected, all the zeros of the function $F(\theta)$ located within the search rectangle will have been found.

FIGURE 13
Phase contour behaviour near a zero of $F(\theta)$



————— Phase contour in the neighbourhood of θ_0
 - - - - - Phase contour beyond the neighbourhood of θ_0 0684-13

FIGURE 14
Mode finding method for the function $F(\theta)$



0684-14

The location of a zero is evident by the intersection of phase contours (see Fig. 13). Therefore, the intersection of the 0° or 180° phase contour with any other phase contour locates a zero of $F(\theta)$. The other phase contour chosen for this purpose is the 90° or 270° phase contour, again chosen for simplicity, as these contours are easily recognized, occurring when $\text{Re}(F) = 0$. While a 0° or 180° phase contour is being traced $\text{Re}(F)$ is also examined at the corners of each mesh square to locate a $\text{Re}(F)$ sign change which indicates that a 90° or 270° phase contour has entered the mesh square. Such an occurrence indicates that a zero is probably within that mesh square or perhaps within an adjacent mesh square. Once a mesh square is known to contain a zero, a more precise location of the zero is obtained by an interpolation scheme which employs both the magnitude and phase of the function $F(\theta)$. Following this a Newton-Raphson iteration pinpoints the location of the zero.

The Newton-Raphson procedure is to use each of the eigenangle solutions, θ_n , as obtained from the “MODESRCH” grid as a starting solution θ_0 to equation (6) where $F(\theta) = 0$. The function is then re-evaluated for $\theta_0 + \delta\theta$ and the correction to θ_0 found from the equation:

$$\Delta\theta = \frac{F(\theta_0) \delta\theta}{F(\theta_0 + \delta\theta) - F(\theta_0)} \quad (14)$$

The correction determined by equation (14) is then evaluated and the process repeated until the quantities $|\Delta\theta_r|$ and $|\Delta\theta_i|$ are reduced to within a pre-assigned tolerance. The subscripts r and i denote the real and imaginary parts, respectively.

4 Calculation of field strength

4.1 Required parameters

With the eigenangles, θ_n , known, the following quantities of physical interest are readily calculated.

$$\text{Phase velocity at the ground} \quad V = \frac{c}{K(\sin\theta_n)_r} \quad (15)$$

$$\text{Attenuation constant at the ground (dB/Mm):} \quad \Gamma = -8.6859 k K(\sin\theta_n)_i \quad (16)$$

where:

$$\text{Vacuum speed of light:} \quad c = 2.997928 \times 10^5 \text{ km/s}$$

$$K = \left(1 + \frac{\alpha h}{2}\right) \quad (17)$$

$$\alpha = 2/a = 3.14 \times 10^{-4} / \text{km} \quad (18)$$

Using the geometry of Fig. 12 the direction of stratification is the z direction and direction of propagation is in the x - z plane. The direction of z is taken as positive into the ionosphere. Positive x is the direction of propagation and y is normal to the plane of propagation. Thus, the fields exhibit no y dependence and a dependence on x of the form $\exp(-ik \sin\theta_x)$ where k is the magnitude of the free-space propagation vector and θ is the angle between the direction of the propagation vector and the z direction at a point in the stratified medium where the modified index of refraction is unity. All field quantities are assumed to have an $\exp(i\omega t)$ dependence where ω is the angular frequency.

The modal excitation factor and the modal height gain functions are two parameters needed in computing electric field strengths. The excitation factor formulae are summarized in Table 2. The column headings only apply to excitation of the electric field components E_z , E_y and E_x and the row headings apply to excitation by a vertical dipole (λ_V), horizontal dipole end on (λ_E) and a horizontal dipole broadside (λ_B).

TABLE 2

Excitation factors

Field component	E_z	E_y	E_x
Exciter			
λ_V	$B_1 \frac{(1 + \bar{R}_{\parallel})^2 (1 - \bar{R}_{\perp} \bar{R}_{\perp})}{\bar{R}_{\parallel} D_{11}}$	$\frac{-B_1}{S} \frac{\bar{R}_{\perp} (1 + \bar{R}_{\parallel}) (1 + \bar{R}_{\perp})}{D_{12}}$	$\frac{B_1}{S} \frac{(1 + \bar{R}_{\parallel})^2 (1 - \bar{R}_{\perp} \bar{R}_{\perp})}{\bar{R}_{\parallel} D_{11}}$
λ_E	$B_2 \frac{(1 + \bar{R}_{\parallel})^2 (1 - \bar{R}_{\perp} \bar{R}_{\perp})}{\bar{R}_{\parallel} D_{11}}$	$\frac{-B_2}{S} \frac{\bar{R}_{\perp} (1 + \bar{R}_{\parallel}) (1 + \bar{R}_{\perp})}{D_{12}}$	$\frac{B_2}{S} \frac{(1 + \bar{R}_{\parallel})^2 (1 - \bar{R}_{\perp} \bar{R}_{\perp})}{\bar{R}_{\parallel} D_{11}}$
λ_B	$B_2 \frac{\bar{R}_{\perp} (1 + \bar{R}_{\perp}) (1 + \bar{R}_{\parallel})}{D_{12}}$	$\frac{-B_2}{S} \frac{(1 + \bar{R}_{\perp})^2 (1 - \bar{R}_{\parallel} \bar{R}_{\parallel})}{\bar{R}_{\perp} D_{22}}$	$\frac{B_2}{S} \frac{\bar{R}_{\perp} (1 + \bar{R}_{\perp}) (1 + \bar{R}_{\parallel})}{D_{12}}$

R and \bar{R} represent, respectively, elements of the reflection matrix looking into the ionosphere and towards the ground from the same level d within the guide. B_1 and B_2 are given by:

$$B_1 = \frac{S^{5/2}}{\left. \frac{\partial F}{\partial \theta} \right|_{\theta = \theta_n}} \quad B_2 = -\frac{B_1}{S} \quad (19)$$

where S is the sine of the eigenangle and the denominator is the derivative of the modal equation at the eigenangle, θ_n .

The excitation factors must be supplemented with definitions of the height gains.

The field strength calculations can be made for electric dipole exciters of arbitrary orientation located at any height within the guide. Thus, air-to-air, ground-to-air or air-to-ground VLF/LF propagation problems involving a horizontally inhomogeneous waveguide channel may be treated. Figure 15 shows the dipole orientation relative to the propagation geometry in which the z axis is always normal to the curved Earth surface. The angles γ and φ measure the orientation of the transmitter relative to the x, y, z coordinate system.

From Fig. 15, $\gamma = 0^\circ$ represents the excitation from a vertical dipole while $\gamma = 90^\circ$ gives the excitation from a horizontal dipole. Also φ is the angle between the direction of the horizontal dipole and the direction of propagation. Explicitly, $\varphi = 0$ represents end fire and $\varphi = 90^\circ$ represents broadside launching.

4.2 WKB and horizontally homogeneous mode sums

In addition to the vertical inhomogeneity of the ionosphere the guide may exhibit horizontal inhomogeneity. In particular, variability in propagation constants along the great circle path of propagation can result from either horizontal variability of the ionosphere, from variability of the ground conductivity and/or permittivity, as well as from variations in the geomagnetic field strength or orientation. In instances for which the Earth ionosphere waveguide cannot be considered as horizontally homogeneous along the propagation path, a WKB form of the mode sum is used. This model is accurate when changes in the modal parameters are sufficiently gradual along the path.

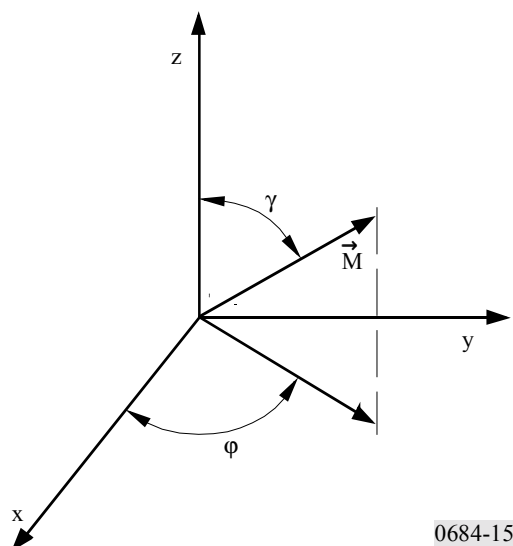
In terms of the excitation factors and height gains, the WKB mode sum equations may be written as a function of propagation distance.

If the propagation path may be considered as horizontally homogeneous along its entire length, the equation becomes much simpler:

$$\left(\lambda \frac{T}{V} = \lambda \frac{R}{V}\right), \left(\lambda \frac{T}{B} = \lambda \frac{R}{B}\right) \text{ and } \left(\lambda \frac{T}{E} = \lambda \frac{R}{E}\right). \quad \text{Also } \left(\bar{S} \frac{T}{n} = \bar{S} \frac{R}{n}\right) \quad (20)$$

and may be used to compute the fields for multimode propagation at VLF and LF. These equations may also be used for ELF. However, because of the small attenuation rates which prevail in the lower ELF band, significant interference between the long and short path signals can occur.

FIGURE 15
Dipole \vec{M} orientation within the waveguide where γ is the inclination and ϕ the azimuthal orientation



0684-15

4.3 Mode sums using mode conversion

For those propagation conditions where the properties of the Earth-ionosphere waveguide can not be considered as slowly varying, mode conversion techniques must be utilized. Examples, where mode conversion procedures are required for calculating field strengths, are for transmissions across the daytime-night-time terminator region or when the propagation path consists of large changes in ground conductivity, such as the transition from land to sea. The mode conversion model allows for an arbitrary number and order of modes on each side of the waveguide discontinuity. This model also allows for the calculation of the horizontal, as well as the vertical, component of the electric field at an arbitrary height in the waveguide.

A mode conversion program (see references given in AGARDograph No. 326, ed. J. H. Richter, p. 40-62, 1990) is based on the slab model shown in Fig. 16. Invariance in the y direction is assumed and reflection from the horizontal inhomogeneity is neglected. Subject to these assumptions and to the assumption of a unit amplitude wave in mode k incident in the transmitter region (slab NTR) the generalized mode conversion coefficient a_k^p for the p -th slab associated with

conversion from the k -th to the j -th mode expressed in terms of the coefficients for the previous $(p + 1)$ -th slab may be written in the form:

$$\sum_{j=1}^j a_{ik}^p I_{n,j}^{p,p} = I_{n,k}^{p,p+1} \quad \text{for } p = NTR - 1$$

$$= \sum_{j=1}^j a_{jk}^{p+1} \left[-ik S_j^{p+1} (x_p - x_{p+1}) \right] I_{n,k}^{p,p+1} \quad \text{for } 1 \leq p < NTR - 1$$
(21)

where:

$$i = (-1)^{1/2}$$

k : free-space wave number

S_j : sine of the j -th eigenangle for the p -th slab

j : total number of modes assumed to be important in the total field determinations.

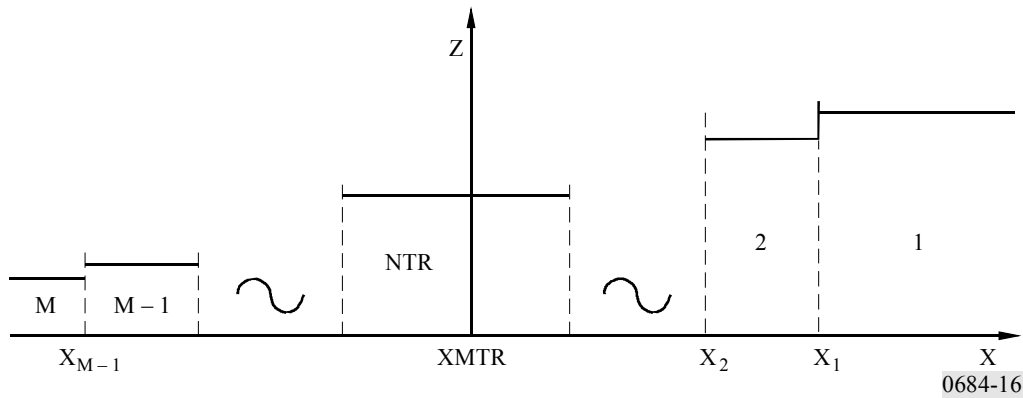
Critical for the solution of the system of equations (21) is the evaluation of the integral:

$$I_{j,k}^{m,p} = \int_{-\infty}^{\infty} A_j^{mt} \cdot G_k^p dz$$
(22)

where the t denotes the adjoint factor and G^p a four-element column matrix of height gains for the y and z components of the electric and magnetic field strength of the k -th mode in the p -th slab.

The term A_j^m is a four-element column matrix of height gains for an appropriate adjoint waveguide.

FIGURE 16
Mode conversion model



Again, as in the case of the WKB mode sum procedure, the field-strength calculations can be made for electric dipole exciters of arbitrary orientation located at any height within the guide. Thus,

air-to-air, ground-to-air or air-to-ground VLF/LF propagation problems in a horizontally inhomogeneous waveguide channel may be treated.

Two distinct options are available with the mode conversion procedure. One is for field calculations (amplitude and phase) as a function of range for a fixed location of the horizontal inhomogeneity. The second allows for field calculations at a distinct receiving point along a great circle path as a function of position of the horizontal inhomogeneity (this option is useful only if the ground conductivity and the geomagnetic parameters are invariant over the path). Amplitude is expressed in dB above a microvolt per metre for a one kilowatt radiator and phase in degrees relative to free space.

4.4 Ionospheric parameters

The required ionospheric parameters needed to compute ELF/VLF/LF field strength values are the following profiles, which are functions of ionospheric height, Z . These are electron density profile, positive and negative ion density profiles, electron-neutral particle collision frequency profile and positive and negative ion-neutral particle collision frequency profiles.

A convenient parameter based on the above profiles is the ionospheric conductivity ω_r , which is a function of height, Z . This parameter is given by:

$$\omega_r(Z) = \frac{\omega_p^2(Z)}{\nu(Z)} = \frac{q^2}{\epsilon_0} \left[\frac{N_e(Z)}{m_e \nu_e(Z)} + \frac{N_+(Z)}{m_+ \nu_+(Z)} + \frac{N_-(Z)}{m_- \nu_-(Z)} \right] \quad (23)$$

where:

- $\omega_p(Z)$: plasma frequency
- q : electron charge
- ϵ_0 : permittivity of free space
- ν_e : electron-neutral particle collision frequency (s^{-1})
- ν_+ : positive ion-neutral particle collision frequency (s^{-1})
- ν_- : negative ion-neutral particle collision frequency (s^{-1})
- N_e : electron density (cm^{-3})
- N_+ : positive ion density (cm^{-3})
- N_- : negative ion density (cm^{-3})
- m_e : mass of the electron
- m_+ : mass of the positive ions
- m_- : mass of the negative ions.

For most cases of propagation at VLF or LF, only the electron density profile and electron-neutral particle collision frequency profile need to be considered. In this instance, the conductivity parameter $\omega_r(Z)$ may be considered of exponential form:

$$\omega_r(Z) = \omega_0 \exp [\beta (Z - H')] \quad (24)$$

where:

- β : gradient parameter in inverse height units, and
- H' : reference height.

The ionospheric parameters needed as inputs to the multimode computer programs, then, are the electron density profile and the effective electron-neutral particle collision frequency profile. These terms may be assigned exponential relationships with height and are identified by the terms β (km^{-1}) and H' (km).

The value of the electron density $N(Z)$, (el/cm^3) is calculated as a function of height Z (km) by the equation:

$$N(Z) = \{1,43 \times 10^7 \times \exp(-0,15 H')\} \{ \exp(\beta - 0,15)(Z - H') \} \quad \text{el}/\text{cm}^3 \quad (25)$$

The collision frequency profile for the computations is:

$$\nu(Z) = \nu_0 \exp(-\alpha Z) \quad (26)$$

where:

Z : height (km)

ν_0 : 1.82×10^{11} collisions/s

α : 0.15 km^{-1} .

This combination of electron density and collision frequency gives an ionospheric conductivity profile given by:

$$\omega_r(Z) = 2.5 \times 10^5 \exp[\beta(Z - H')] \quad (27)$$

The usefulness of this simple ionospheric model is a result of its ease of application and its success in modelling experimentally measured data. The determination of the values of the β and H' parameters is achieved by comparing measured data with theoretical calculations, adjusting the parameters in the latter until acceptable agreement is obtained. The most straightforward method of comparison is obtained when the measured data are collected at a large number of points along a great circle propagation path which includes the transmitter. The easiest way to collect such data is aboard an aircraft.

In general, the ionospheric models determined from the above procedure must be considered to represent an averaged ionosphere since the modelling assumes that the ionosphere was static during any aircraft flight period. The data fitting procedure attempts to find a calculated pattern of amplitude as a function of distance which agrees with the large scale pattern of the measured data. Thus, many small amplitude variations are averaged. It is possible that profiles of more complex forms than the exponential could be found to produce a better fit to measured data in some instances, but since the propagation paths considered are quite long, any profile determined to produce a best fit to the data is really an average profile for the total path.

Analysis of the available measured data suggests the following parameters for VLF/LF predictions. For daytime use $\beta = 0.3$ and $H' = 74$, for all latitudes, and all seasons. The night-time ionosphere is more complicated in that β varies linearly with frequency from 0.3 at 10 kHz to 0.8 at 60 kHz. The low- and mid-geomagnetic latitude night-time ionosphere is characterized by an H' of 87 km, while the polar ionosphere has an H' of 80 km. Values of these transmission parameters at 30 kHz are found in Table 3. This table illustrates the transitions as they would be defined along a hypothetical path which traverses the pole from day to night.

TABLE 3

Ionospheric profile transition parameters at 30 kHz

Solar zenith angle, χ	β	H' (km)	Magnetic dip angle, D
$\chi < 90.0$	0.3	74.0	$D < 70$
$90.0 < \chi < 91.8$	0.33	76.2	$70 < D < 72$
$91.8 < \chi < 93.6$	0.37	78.3	$72 < D < 74$
$93.6 < \chi < 95.4$	0.40	80.5	$74 < D < 90$ (Pole)
$95.4 < \chi < 97.2$	0.43	82.7	$72 < D < 74$
$97.2 < \chi < 99.0$	0.47	84.4	$70 < D < 72$
$99.0 < \chi < \text{(night)}$	0.50	87.0	$D < 70$

The characteristic relationship, as a function for some exponential profiles is illustrated in Fig. 17 for daytime conditions and in Fig. 18 for night-time conditions.

For propagation at ELF, suggested electron and ion density profiles are shown in Fig. 19.

Tables of suggested electron and ion collision profiles for ELF are given in Tables 4 and 5.

FIGURE 17

Daytime electron density profiles and collision frequency profile

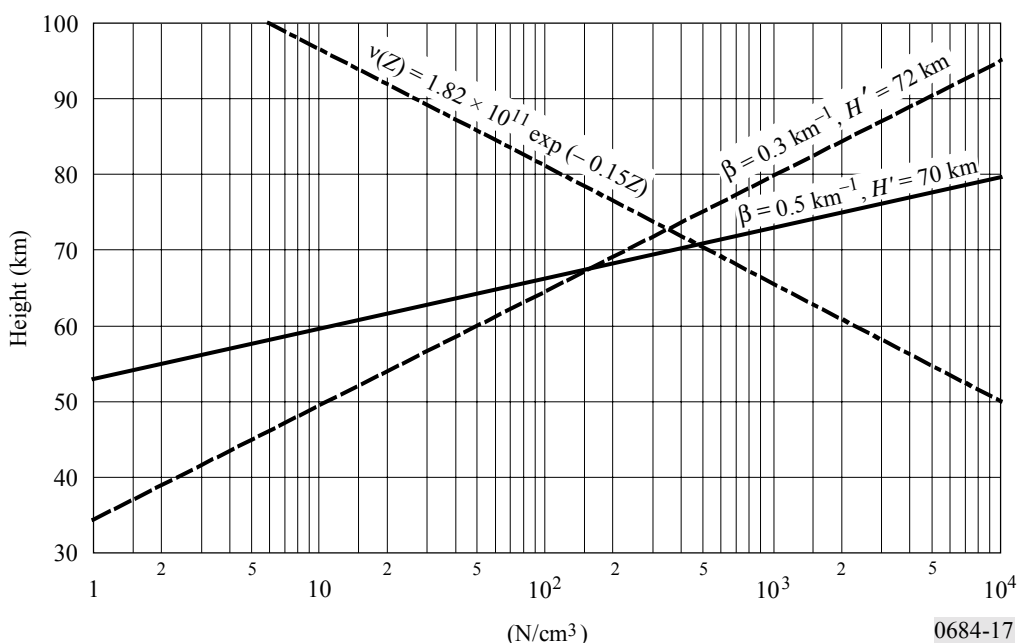


FIGURE 18

Night-time electron density profiles and collision frequency profile

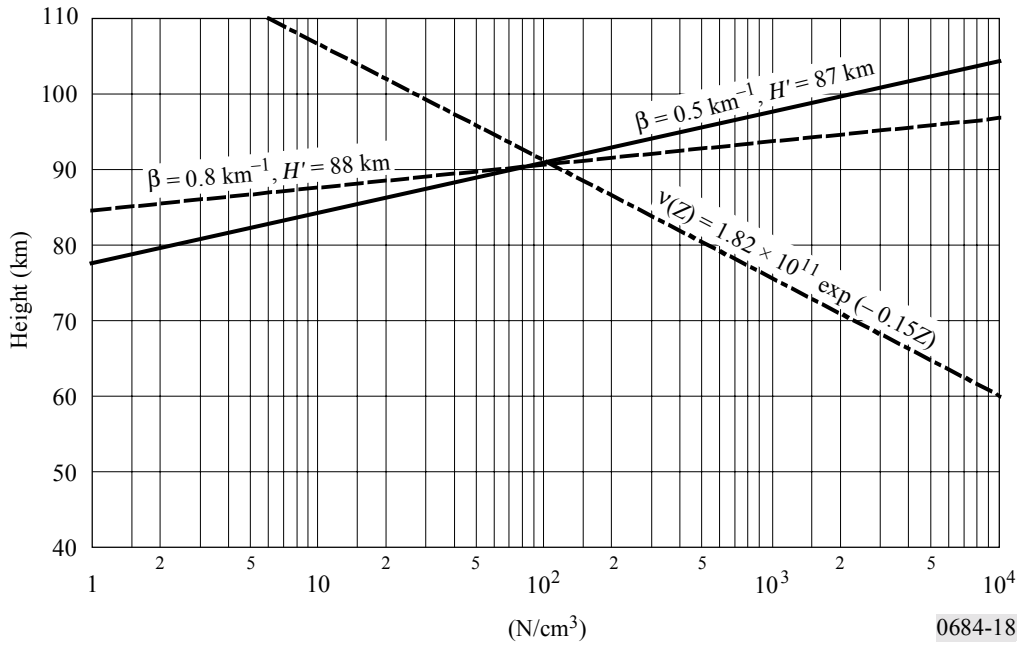
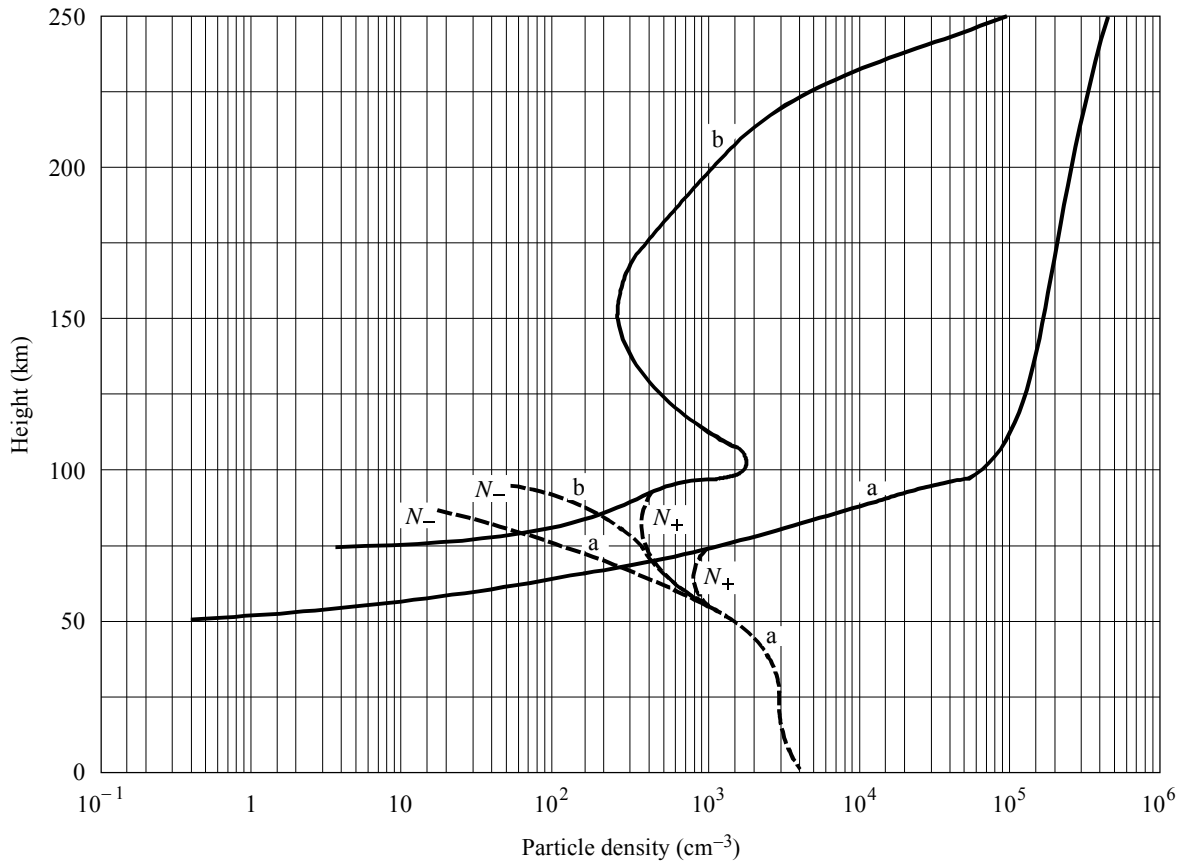


FIGURE 19

Ambient day and night constituent profiles



- Electrons
- - - Ions
- a: day
- b: night

TABLE 4

Daytime ionospheric electron and ion collision frequency (s^{-1}) versus height

Height (km)	Electrons	Positive ions	Negative ions
260	6.6×10^2	1.02	1.02
230	5.3×10^2	2.00	2.00
210	4.8×10^2	3.10	3.10
200	5.0×10^2	4.00	4.00
180	6.0×10^2	1.30×10	1.30×10
170	8.0×10^2	2.40×10	2.40×10
150	1.6×10^3	9.00×10	9.00×10
120	1.0×10^4	6.00×10^2	6.00×10^2
100	3.9×10^4	1.60×10^4	1.60×10^4
0	4.3×10^{11}	2.14×10^{10}	2.14×10^{10}

TABLE 5

Night ionospheric electrons and ion collision frequency (s^{-1}) versus height

Height (km)	Electrons	Positive ions	Negative ions
250	1.05×10^2	4.50×10	4.50×10
225	3.50×10	9.00×10	9.00×10
220	3.00×10	1.00	1.00
210	3.30×10	1.30	1.30
200	4.50×10	2.00	2.00
150	1.60×10^3	4.50×10	4.50×10
120	1.00×10^4	3.00×10^2	3.00×10^2
100	3.90×10^4	8.00×10^3	8.00×10^3
0	4.30×10^{11}	1.07×10^{10}	1.07×10^{10}

4.5 Geomagnetic and geophysical parameters

Other parameters needed for the calculation of ELF/VLF/LF signal levels are those which describe the orientation and strength of the Earth's magnetic field along the propagation path, as well as those parameters which give the value of the Earth's complex dielectric constant as a function of propagation frequency.

The parameters which describe the Earth's magnetic field are the magnitude of the geomagnetic field, the magnetic azimuth (in degrees east of North) of the propagation direction, and the dip angle measured from the horizontal (co-dip) of the magnetic field vector. These parameters change along the propagation path and these changes are incorporated in the WKB or mode conversion formulations.

The complex relative permittivity of the Earth, N_g , is given by:

$$N_g = \varepsilon/\varepsilon_0 - i \frac{\sigma}{\omega \varepsilon_0} \quad (28)$$

where:

σ : ground conductivity

$\varepsilon/\varepsilon_0$: relative ground permittivity

ε_0 : permittivity of free space

ω : angular propagation frequency.

Table 1 gives recommended values for these parameters.

5. Discussion

The wave-hop and waveguide mode methods described in detail in this Recommendation should be used, until better methods are available, to predict field strengths for frequencies below about 150 kHz. While the waveguide mode propagation program described in detail in this Recommendation can be used to predict field strength at ELF (50 Hz to 3 000 Hz), simpler methods have been developed for the low frequency part of this band.

A brief discussion of the accuracy of the methods is given in Annex 2. Some interesting results using the waveguide mode propagation prediction program are given in Annex 3, to illustrate the usefulness of this program.

ANNEX 1

Example of a complete calculation of field in amplitude and phase using the wave-hop method of § 2

It is required to calculate the summer daytime expected field during solar cycle minimum under the following conditions using short vertical dipole transmitting and receiving antennas:

Length of path	$d = 1\,911$ km
Frequency	$f = 80$ kHz
Transmitting location on land	$\left\{ \begin{array}{l} \sigma = 2 \times 10^{-3} \text{ S/m} \\ \varepsilon = 15 \varepsilon_0 \end{array} \right.$

Receiving location on sea water $\left\{ \begin{array}{l} \sigma = 5 \text{ S/m} \\ \epsilon = 80 \epsilon_0 \end{array} \right.$

Radiated power $p_t = 0.4 \text{ kW}$

The successive stages of the calculation are as follows:

Stage	Parameters	Figures	Terms calculated	Values
1	$p_t = 0.4 \text{ kW}$		$V_u = 300\sqrt{0.4}$	= 190 V
2	$d = 1\,911 \text{ km}$	2	ψ i	$\approx -0.36^\circ$ = 81°
3	$\psi = -0.36^\circ$	8	F_t	= 0.36
4	$\psi = -0.36^\circ$	7	F_r	= 0.67
5	$d = 1\,911 \text{ km}$ $c = 3 \times 10^5 \text{ km/s}$	4	$L - d$ $L = 1\,911 + (46 \times 10^{-6} \times 3 \times 10^5)$	= 46 μs = 1 925 km
6	$d = 1\,911 \text{ km}$	5	D	= 2.16
7	$f = 80 \text{ kHz}$ $i = 81^\circ$		$f \cos i = 80 \cos 81^\circ$	= 12.5 kHz
8	$f \cos i = 12.5 \text{ kHz}$ solar cycle minimum day (summer)	10	$\ R\ $	= 0.11
9			E_s	= $11.4 \times 10^{-3} \text{ mV/m}$
10	$h = 70 \text{ km}$ (day) $h = 90 \text{ km}$ (night) $d = 1\,911 \text{ km}$ (1 hop)	4	Differential time delay	= 67 – 47 = 20 μs = 1.6 cycle (i.e. 576°) at 80 kHz

ANNEX 2

Accuracy of the methods

The wave-hop method still needs to be verified on a worldwide basis, since this method has largely been based on observations at middle latitudes in ITU Regions 1 and 2. The method has however been found to predict median field strengths with good accuracy in high latitudes in Region 2. The wave-hop method can be used for LF for frequencies between about 60 kHz and 150 kHz.

When using this method account needs to be taken of ground-wave propagation (Recommendation ITU-R P.368), and due allowance taken of the vertical plane antenna factor, using information

given in this Recommendation and in the ITU-R Handbook on the ionosphere and its effects on radiowave propagation.

The waveguide mode method can be used to predict field strengths up to about 60 kHz, using the value 0.3/74 for the ionospheric parameters β/H' for day-time paths, until additional results taking into account the variation with season, solar activity and frequency can be obtained. A more detailed model for night-time, which is a function of frequency and latitude, is given in this Recommendation.

Since the lower boundary of the waveguide is the Earth, a conductivity map of the world (e.g. Recommendation ITU-R P.832) needs to be a part of a program developed for worldwide application. The ground conductivity map currently used for the long-wave waveguide prediction program currently in use in the United States of America and Canada is largely based on geological features.

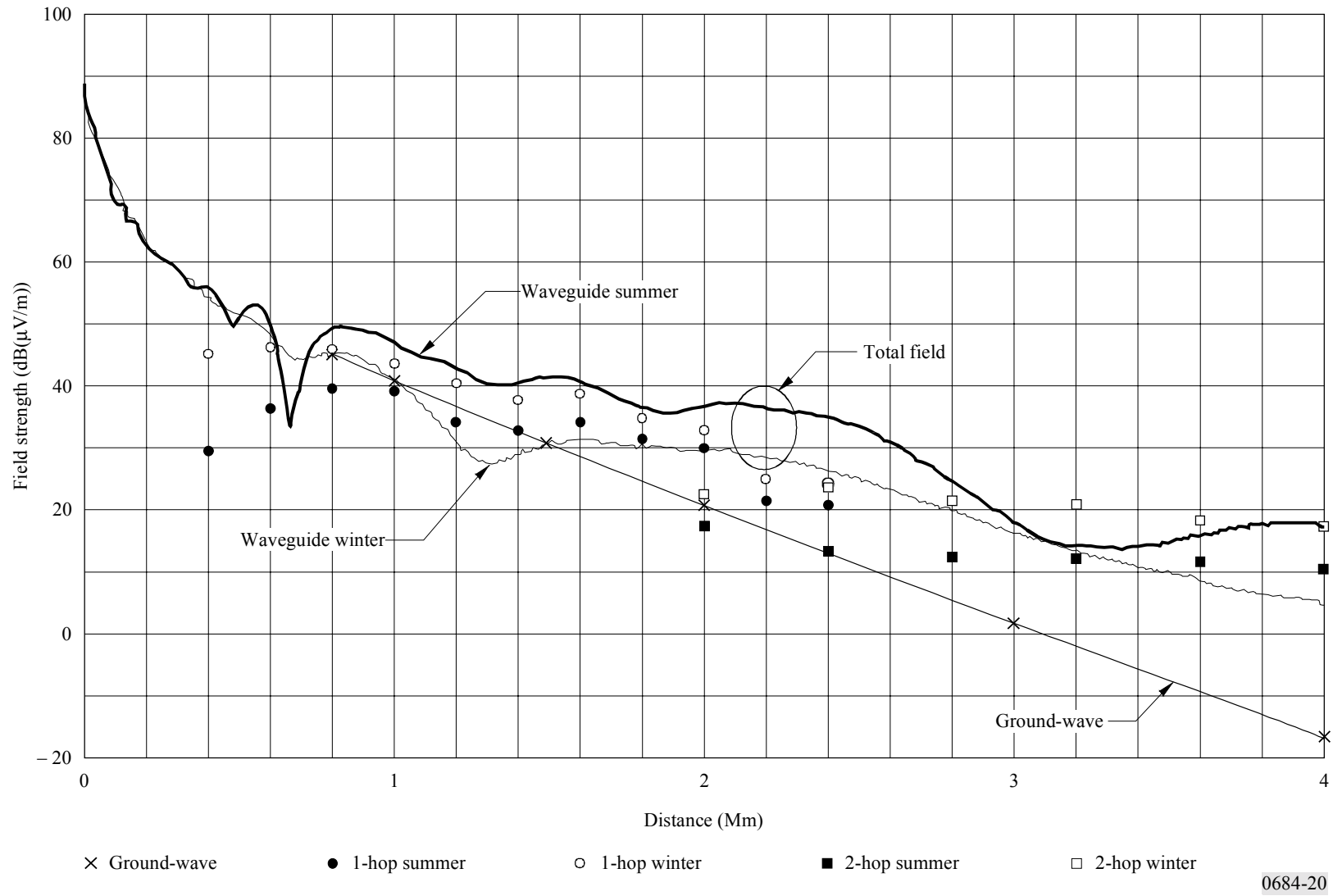
Alternative methods to calculate night-time field strengths at LF, and above to 1 705 kHz, are given in the ITU-R Handbook on the ionosphere and its effects on radiowave propagation. An intercomparison of results obtained by the method proposed in this Recommendation (the wave-hop method) should be made. Certainly field strengths predicted by the alternative methods should be consistent for frequencies and distances which are the same.

In daytime, LF sky waves propagating in winter are at least 20 dB stronger than in summer and may be only 10 dB below night-time values. At night, LF sky waves are stronger in summer and winter and are weaker in spring and autumn. Midday sky-wave field strengths at LF can be surprisingly strong, particularly in winter months. Daytime annual median field strength is typically 20 dB lower than its counterpart at night. For additional guidance, see also the above-mentioned Handbook.

The wave-hop method can be used to predict MF field strengths and LF field strengths down to a frequency of about 60 kHz. The waveguide mode method can be used to predict VLF and LF field strengths, up to a frequency of about 60 kHz. Daytime field strength predicted by the two methods for a frequency of 60 kHz are shown in Fig. 20 (unfortunately for this comparison there are no measured data to compare). The continuous lines labelled summer and winter are calculated by the waveguide mode prediction program (using parameters for β/H' given in Report ITU-R P.895). The open and closed circles are respectively the summer and winter field strengths calculated by the wave-hop method. No attempt is made to smooth the data in the over-lap distance range where the one-hop sky wave is cut off and the two-hop sky-wave dominates. The ground-wave is shown separately.

The waveguide mode method calculates the total field, ground and sky-wave. The wave-hop method estimates the amplitude of the sky-wave alone. Therefore for comparison, the ground-wave field strength must be included in the wave-hop method. The waveguide mode method was used to predict field strength versus distance for a real path from a hypothetical transmitter at Vancouver, for a West-to-East path across Canada and the United States of America. The ground conductivity is variable along this path. The wave-hop method assumed average ground, conductivity 3 mS/m along the path.

FIGURE 20



0684-20

The difference between summer and winter daytime field strengths according to the wave-hop method decreases with decrease in effective frequency ($f \cos i$). The waveguide mode propagation prediction program used for this intercomparison predicted the opposite seasonal variation. The program used parameters (β/H') given in Report ITU-R P.895. Hence the caution noted above. The seasonal variation cannot be predicted and 0.3/74 for the parameters β/H' is recommended for all seasons.

ANNEX 3

Some example calculations using the waveguide mode method

This Annex includes some calculations to illustrate that the waveguide propagation program (see § 4.3) predicts field strengths that are in accord with expectation concerning path features (ground conductivity) and path orientation with respect to the magnetic field.

A Northern Hemisphere coverage pattern for a hypothetical VLF transmitter in central Canada is shown in Fig. 21. The calculations (field strength (dB(μ V/m))) are for 1 kW radiated power at a frequency of 24 kHz. Notice that in general the features agree with expectation. Propagation from East-to-West is better than from West-to-East; and notice the interesting anomaly in the field strength contours which result from the very low conductivity of Greenland. Notice the increased field strengths due to the good ground conductivity of the sea water in the Hudson Bay, compared with the surrounding poor conductivity of Arctic terrain.

Another example follows to show that the ground conductivity along the whole of the propagation path is important. For the wave-hop method only the ground in the vicinity of the transmitting and receiving antennas is important. In Figs. 23 and 24 we show a detailed field strength vs. distance prediction for three frequencies, 15, 25 and 35 kHz for a hypothetical path from Halifax across the poor conductivity land of the Laurentian Shield and over the Ungava Peninsula (the path is marked in Fig. 22). The poor ground conductivity for this path, across the Laurentian Shield in Canada, affects the frequencies differently. A transmit frequency of 25 kHz is the best frequency for daytime propagation for this path (Fig. 23). The frequency differences are less marked at night (see Fig. 24).

Clearly the details given in these Figures could not be anticipated without the availability of a propagation prediction program.

FIGURE 21
Field strength contours (dB(μ V/m)) for 1 kW radiated power, for a hypothetical transmitter located in central Canada.
(Frequency 24 kHz, for a summer day)

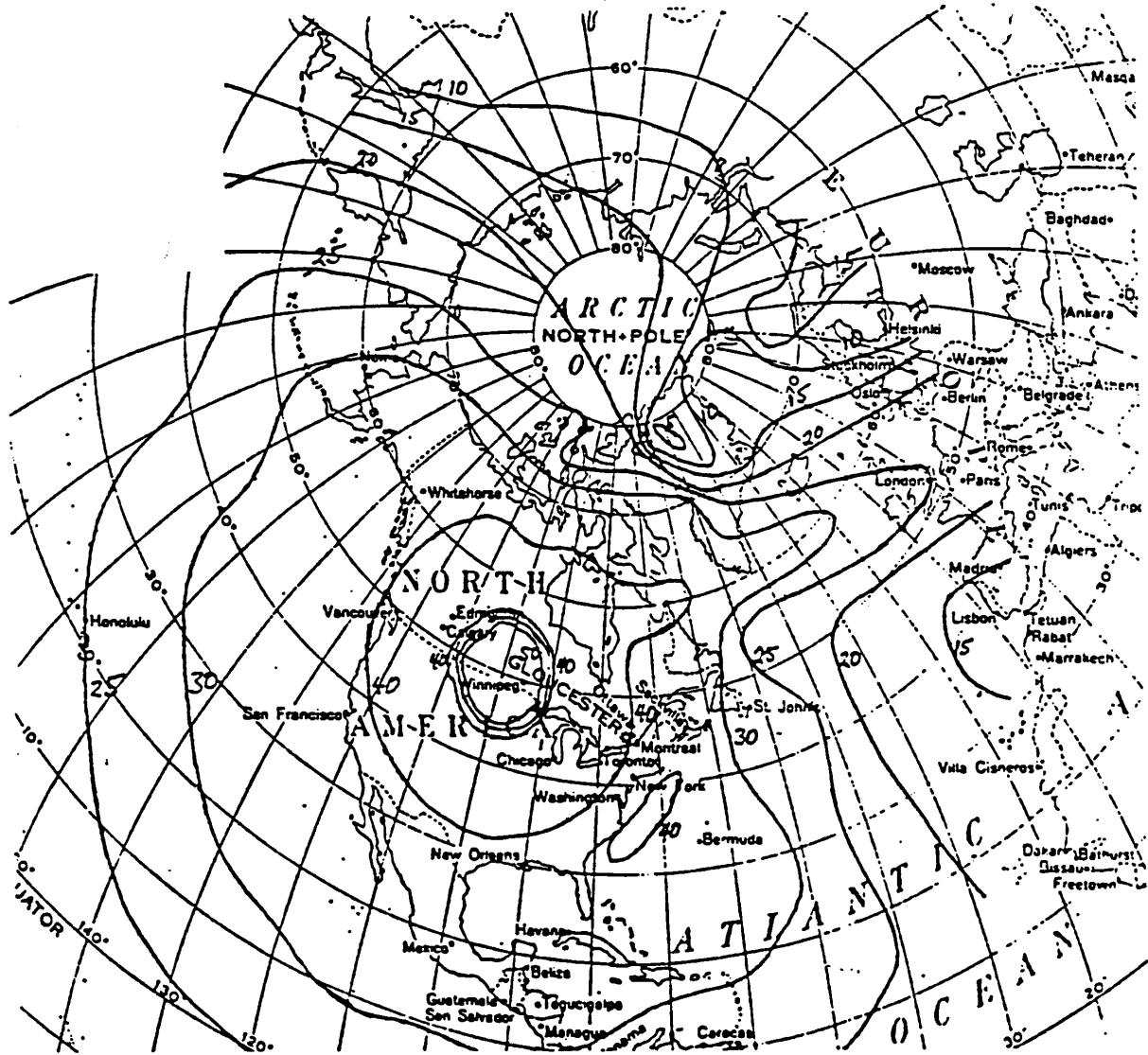


FIGURE 22
VLF ground conductivity map for Canada and the Arctic (mS/m)

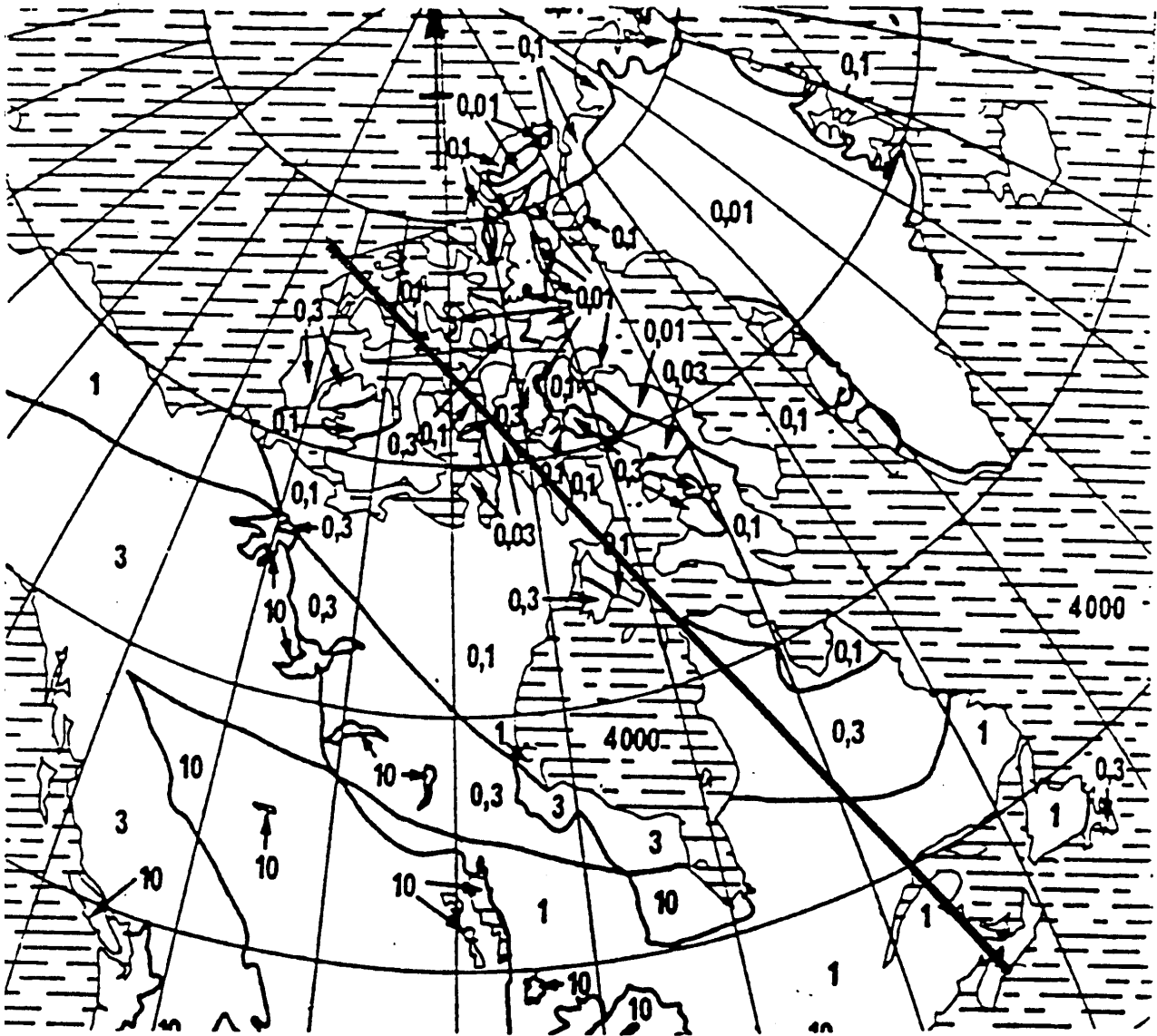


FIGURE 23

Field strength vs distance at a bearing of 340° N for 1 kW radiated power from a hypothetical transmitter located at Halifax, for 3 frequencies, for a summer day. The transmission path is drawn on Fig. 22

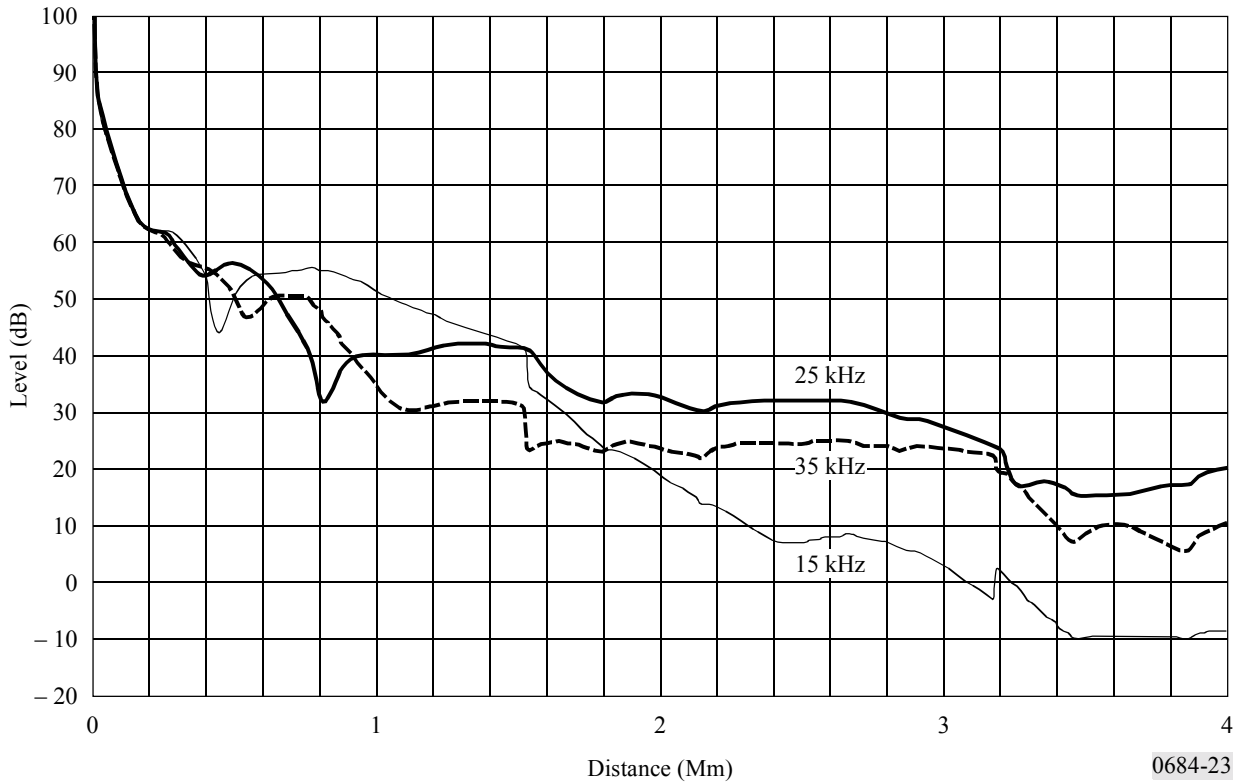


FIGURE 24

Field strength vs distance at a bearing of 340° N for 1 kW radiated power from a hypothetical transmitter located at Halifax, for 3 frequencies, for a summer night. The transmission path is drawn on Fig. 22

